Chapter 2
High-Temperature Superconductors. Overview

2.1 General Remarks on Type-II Superconductors

High-temperature superconductors placed in the center of our research are the type-II superconductors. Therefore, their properties and superconductivity mechanisms are considered in more detail. The term type-II superconductors was first introduced by Abrikosov in his classical paper [4], where he assumed a detailed phenomenological theory of these materials' behavior, based on the Ginzburg–Landau theory, and explained their magnetic properties. Initially, Abrikosov's theory was greeted with certain skepticism: so much out of the ordinary was in its predictions. However, at the next development of physics of superconductors this theory obtained numerous experimental supports. Finally, several years later it was accepted in total, when it consequently explained the complex behavior of superconducting alloys and compounds, in particular the very high critical fields of some materials. As it has been noted for type-II superconductors, the energy of an interface between a normal and a superconducting region $\sigma_{ns} < 0$. Total displacement of external field from superconductor does not lead to a state with the least energy, if the contribution of surface energy of the interface between two phases is significant. Therefore, in this case, the energetically favorable state is that at which superconductor of corresponding shape (any one, besides an infinitely long cylinder placed in a parallel magnetic field) is divided into great number of alternating superconducting and normal regions.

The magnetization curve of a type-II superconductor in the form of a long cylinder, placed in a parallel magnetic field, is shown schematically in Fig. 2.1. As long as the external field is $H < H_{c1}$, the field in the interior of the sample is absent ($B = 0$). At the attainment of the lower critical field $H_{c1} = H_{cm}\kappa^{-1}(\ln\kappa + 0.08)$

I. A. Parinov, *Microstructure and Properties of High-Temperature Superconductors*,
DOI: 10.1007/978-3-642-34441-1_2, © Springer-Verlag Berlin Heidelberg 2012

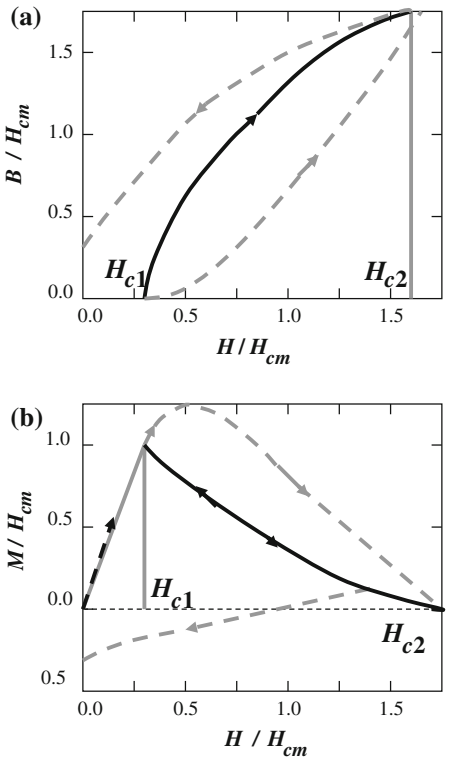

Fig. 2.1 Magnetic induction (**a**) and magnetization (**b**) as a function of applied field in type-II superconductors. *Dotted lines* correspond to impure samples [1006]

[1502], when the Ginzburg–Landau parameter $\kappa \gg 1$, then it becomes to be energetically advantageous the penetration of magnetic field into superconductor.

At the $H_{c1} < H < H_{c2}$, a steadily increasing field penetrates the superconductor in the form of flux lines (vortices). It remains below the external field H, and superconductivity of the sample is not destroyed. At a certain field $H = H_{c2} = \sqrt{2}\kappa H_{cm}$ [4], the field in the interior becomes equal to external field H, and the bulk superconductivity disappears. In contrast to the type-I superconductors, the superconductivity may easily originate in a heterogeneous way in these materials. In this case, the field of the superconductivity initiation H_{c2} may be well above the critical thermodynamic field H_{cm}. Between H_{c1} and H_{c2}, the material has no electric resistance and contains a lattice of flux lines, which can be simplistically treated as normal regions. This is the mixed state, also known as the Schubnikow phase [1570].

In existence of electric field, Lorentz force influences on the vortices. If the vortices are not pinned onto defects or material heterogeneities, then they move and induce electric field, in this case takes place energy dissipation and critical current is equal to zero. If the sample to be in no external magnetic field, then the critical current is defined by equality of the Lorentz force and the pinning force holding the vortices. The anchoring the vortices by impurities (or defects) can lead

to significant hysteresis and even paramagnetization curves, as shown in Fig. 2.1. These material heterogeneities can be formed artificially so increasing the critical current of the flux pinning (the materials with the critical current of the flux pinning $\sim 10^5$ A/cm^2 relate to *rigid superconductors*).

Thus, the above H_{c1} type-II superconductors do not show the Meissner effect. Magnetic field penetrates into these materials in the form of quantized flux lines (vortices), each of which has a normal core, which can be approximated by a long thin cylinder with its axis parallel to the external magnetic field. Inside the cylinder, the order parameter, $\Psi = 0$. The radius of the cylinder is of the order ξ, the coherence length. The direction of the super-current, circulating around the normal core, is such that the direction of the magnetic field, generated by it, coincides with that of the external field and is parallel to the normal core. By this, the vortex current circulates into region with radius of the order λ. The size of this region is by far above a value ξ, because $\lambda \gg \xi$ for type-II superconductors [1502].

Each vortex carries one magnetic flux quantum. Penetration of vortices in the interior of a superconductor becomes thermodynamically favorable at $H > H_{c1}$. Inside the superconductor, the vortices arrange themselves at distances $\sim \lambda$, from each other, so that in the cross-section, they form a regular triangular or square lattice (see Fig. 2.2). This state of superconductor (at $H_{c1} < H < H_{c2}$) is the mixed state, because it is characterized by a partial penetration of the magnetic field in the interior of the sample. Once formed at H_{c1}, the vortex lattice persists at much higher fields. As the external field increases, the lattice period steadily decreases and the density of the vortices rises.

The picture of the mixed state remains before upper critical field H_{c2}, when superconductivity into the specimen volume (excepting only thin surface layer) eliminates completely. At this field occurs failure of Cooper pairs caused by their twisting, because the pair can exist as a single whole until the radius of Larmor precession exceeds the proper size of Cooper pair, ξ. At the field $H = H_{c2}$, the vortex lattice becomes so dense that the distance between the neighboring vortices, that is, the lattice period attains the order ξ. This means that the normal cores of the vortices come into contact with each other and the order parameter Ψ becomes zero over the volume of the superconductor, that is, a second-order phase transition occurs.

2.2 High-Temperature Superconductive Cuprates

2.2.1 Doping of Cuprates

The simplest copper oxide perovskites are insulators. In order to become superconducting, they should be doped by charge carriers. There are two ways to increase the number of charge carriers in cuprates chemically: (i) to substitute metallic atoms in the intermediate planes by higher-valence atoms and/or (ii) to

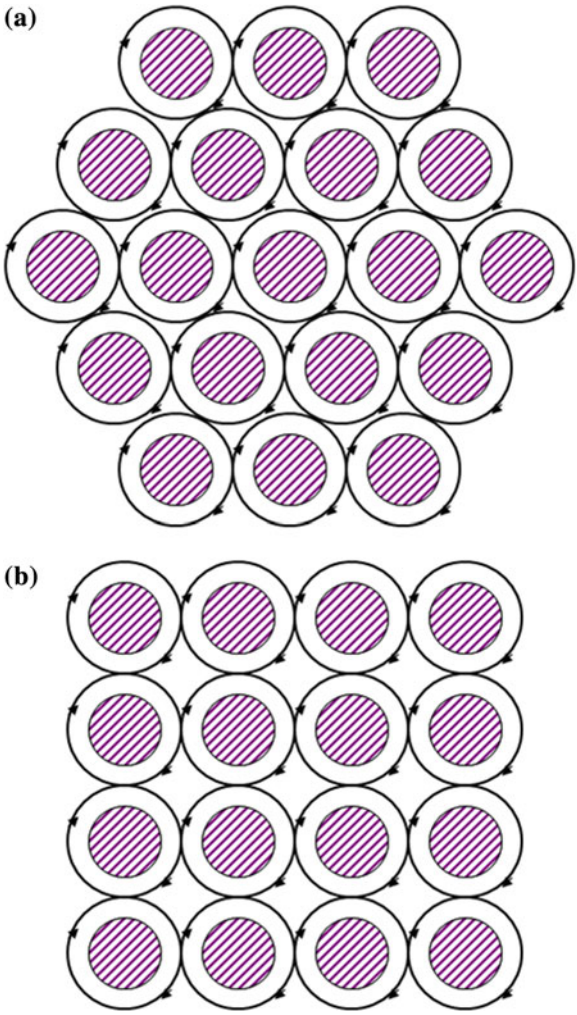

Fig. 2.2 Mixed state of a type-II superconductor. Superconducting vortices form a regular *triangular* (*hexagonal*) (**a**) or *square* (**b**) lattice. Vortex cores (*dashed regions*) are normal

change the number of oxygen atoms. Doping increases the number electrons or holes at the Fermi level. The concentration of charge carriers in HTSC is low ($\sim 5 \times 10^{21}$), in comparison with conventional superconductors ($\sim 5 \times 10^{22} - 10^{23}$). However, due to the large coherence length in conventional superconductors, only a 10^{-4} part of the electrons, located near the Fermi surface, participate in coupling. At the same time, in cuprates, ~ 10 % of all conduction electrons (holes) form the Cooper pairs.

In conventional superconductors, the critical temperature increases monotonically with growth of charge carriers: $T_c(p) \propto p$. In cuprates, this dependence is non-monotonic. In most of hole-doped cuprates (but not in all) the $T_c(p)$ dependence has the bell-like shape and can be approximated as [1399]

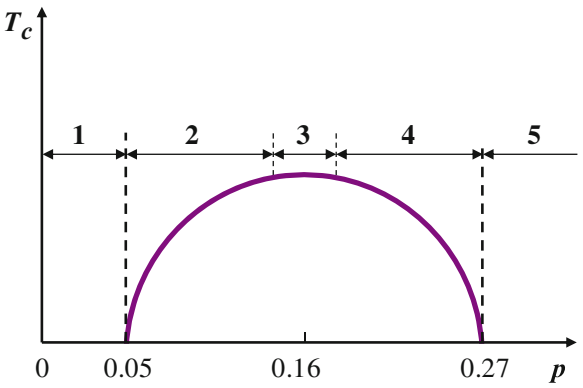

Fig. 2.3 Critical temperature as a function of doping [1201]. Numbers mark the next regions: *1* undoped ($p < 0.05$); *2* underdoped ($0.05 \leq p \leq 0.14$); *3* Optimally doped ($0.14 < p < 0.18$); *4* overdoped ($0.18 \leq p \leq 0.27$), and *5* metalic phase (p > 0.27)

$$T_c(p) \approx T_{c,\,max}[1 - 82.6(p - 0.16)^2], \tag{2.1}$$

where $T_{c,max}$ is the maximum critical temperature for a given compound.

Superconductivity occurs within the limits, $0.05 \leq p \leq 0.27$, which vary slightly in various cuprates. Thus, the different doping regions of the superconducting phase may be chosen such as *the underdoped, optimally doped and overdoped* regions (Fig. 2.3).[1] The insulating phase at $p < 0.05$ is called *the undoped* region, but above 0.27, cuprates become *metallic*.

The ratio between the maximum critical temperatures in hole-doped and electron-doped cuprates is 135 K⁄24 K = 5.6. Obviously, it may be assumed that the electron–hole asymmetry has fundamental character: superconducting hole-doped compounds will always have the critical temperature a few times higher than the same electron-doped superconductors.

In cuprates and in many other compounds with low dimensionality, the distribution of charge carriers is heterogeneous. Moreover, in cuprates, this distribution is heterogeneous in a micro-, as in a macroscopic scale (Fig. 2.4). In the undoped region ($p < 0.05$), doping holes are preferably distributed heterogeneously into CuO_2 planes, and they form dynamical one-dimensional charge stripes (so-called *charge-stripe phase*). In the undoped region, these stripes have diagonal shapes and locate not along –O–Cu–O–Cu– bonds, but along the diagonal –Cu–Cu–Cu– direction, as shown in Fig. 2.4. In undoped cuprates, the concentration of holes is low, but the distance between charge stripes, separated by

[1] For these regions various model representations have been developed. In particular, as one of the models of underdoped cuprates, it is considered so-called *granular superconductivity*. This state realized in the case, when microscopic superconductive grains are divided by non-superconductive regions, through which the grains interact one with others by means of *Josephson tunneling* (as a result, it is stated macroscopic superconducting state). While a structure of HTSC monocrystals is no granular, the theory speaks on that, what at low hole concentration of carriers (underdoped compounds), the holes concentrate into some regions leading to arising isolated between themselves superconductive domains. The granular superconductivity arises owing to the Josephson tunneling between these domains.

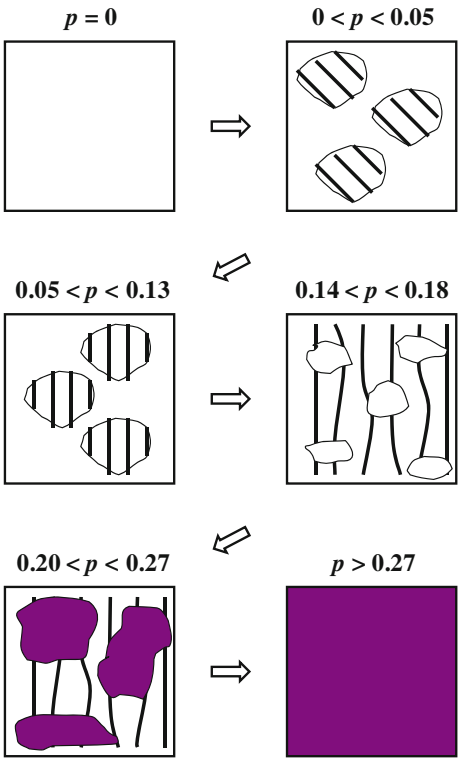

Fig. 2.4 Distribution of charges in CuO_2 planes as function of doping [1201]. The antiferromagnetic and metallic phases are shown in *white* and *gray*, respectively. The *lines* depict charge stripes

two-dimensional insulating antiferromagnetic domains, is large. The charge-stripe phase is distributed heterogeneously: there are two types of small islands, containing either the antiferromagnetic or the charge-stripe phase.

In the underdoped region ($0.05 < p < 0.13$), charge stripes are vertical (or horizontal) and located closer to each other. In this region, the average distance between charge stripes d_s is approximately proportional to $1/p$ and saturates at $p = 1/8$ (Fig. 2.5). Above $p = 1/8$, the distance between stripes is practically constant. As p increases, the concentration of antiferromagnetic regions decreases, but the two types of islands, containing the antiferromagnetic phase and the vertical

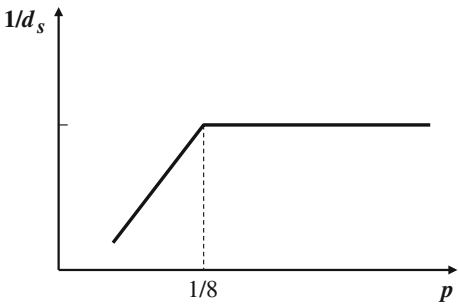

Fig. 2.5 Dependence of incommensurability δ ($\propto 1/d_s$) of spin fluctuations on doping level [1818]

charge-stripe phase, still co-exist. The dynamical charge stripes can move in the transverse direction, and they are *quasi-one-dimensional*. In the near optimally doped region ($p \sim 0.16$) and in the overdoped region ($0.2 < p < 0.27$), the average distance between charge stripes remains almost constant (see Figs. 2.4 and 2.5). Therefore, as the doping level increases, new doped holes cover antiferromagnetic islands, which completely vanish at $p = 0.19$. Above this value, small metallic islands start appearing. Above $p = 0.27$, the charge-stripe distribution becomes homogeneous in two-dimensional CuO_2 planes, and cuprates transform in non-superconducting (normal) metals.

2.2.2 Anderson Phase Diagram of Cuprate Superconductivity

Obviously, that the p–T_c phase diagram presented in Fig. 2.3 is very approximate and not take into account some effects which are characteristic for cuprate superconductivity. Therefore, in this section we consider more complex and probable p–T phase diagram developed by Anderson for superconductive cuprates [43] and presented in Fig. 2.6.

This phase diagram has been developed based on viewpoint on HTSC as a kind of perovskite, key concepts of Mott insulator and super-exchange, Jahn–Teller distortions, antiferromagnetism and *d*-shells. The "plain vanilla" theory—the simple Hubbard model transformed into *t*–*J* model, which was created by Anderson with co-authors (see in some details Sect. 1.6), allows one to understand a behavior of the cuprates in dependence on the doping degree. This theory which

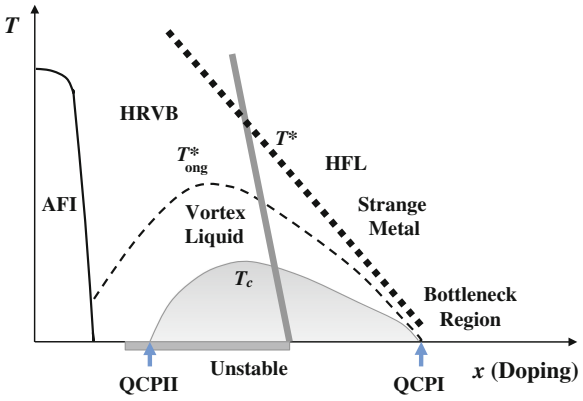

Fig. 2.6 Schematic phase diagram of cuprate superconductivity which is enough general for different materials [43]. Abbreviators design the following: *AFI* Anti-Ferromagnet Insulator, *HRVB* Hidden Resonating Valence Bond, *HFL* Hidden Fermi Liquid, *QCP* Quantum Critical Point; T^* is the pseudogap temperature at which a gap begins to open in the single-particle spectrum, T^*_{ong} is the temperature bound the role of which will be discussed bellow into text

is capable to explain crucial experimental anomalies, in particular tunnel spectra proper for different superconductive cuprates has dealing with the constrained Hilbert space which follows from the requirement of Gutzwiller projection.

In the considered problem, the projective t–J Hamiltonian has two terms, and there are three possible situations defined by doping and temperature changes, namely:

(i) t may dominate (the overdoped case),
(ii) both terms are relevant, but J may be considered as a perturbing interaction (the optimally doped case),
(iii) J is dominant, and determines the shape of the spectrum, but t is also relevant (the underdoped case).

Case (i) applies everywhere above and to the right of the pairing line T^* on the generalized phase diagram (Fig. 2.6) and imagines the energy gap vanishing. In that event, the mean field result of Anderson–Ong [45] implies a jump discontinuity at the Fermi energy. In order to treat this case Anderson used a self-consistent *ansatz* by the same arguments based on momentum and energy conservation which underpin the conventional Fermi liquid [43], while there is not rigorous proof that it is true, the best evidence that it coincides with experiment: fitting laser-excited Angle-Resolved Photoemission Spectroscopy (ARPES) energy distribution curves to shapes derived from this assumption [242]. Then the single-fermion operators acting within the unprojected Hillbert space are the "Hidden Fermi Liquid".[2] They represent true eigen excitations of the system but are not true quasiparticles (they are to be so-called, "pseudoparticles" being true excitations, but not continuously associated to the real electrons and holes of the system). The quasiparticles are three-pseudoparticle operators. They are the physical particles which are exchanged by tunneling or acted on by physical fields. It is the Green's functions of the true quasiparticles which underline all of the phenomena of the "Strange Metal" (sometimes referred to as the "Marginal Fermi Liquid") region of the superconductive cuprate phase diagram. The "linear T" relaxation rates are striking feature of the strange metal. The other idea, namely: the "bottleneck" completes our understanding of this case. A great deal of test data has supported the idea that there are two relaxation rates and two relaxation processes active in this region, characterized by linear T and quadratic T relaxation rates. By using these two concepts Casey has been able to understand the full range of data on the bulk properties available in the strange metal region [241]. The bottleneck process can explain one striking fact on the resistivity: that the "linear T" resistivity often passes without a hitch right through the Mott–Ioffe–Regel "maximum metallic resistivity" [39] without saturating as conventional resistivity in metals does.

Case (ii) develops a true energy gap and due to the optimally doped superconductor can be treated to a fair level of approximation as a simple modified BCS

[2] The general "Hidden" scheme has been presented in [43, 1830].

theory ignoring the incoherent terms caused by projection [45]. In discussing the Fermi liquid, it is introduced the above-pointed pseudoparticles and if they are directly used in deriving the tunneling spectrum, we would find it symmetric. However, the spectra observed for optimally doped HTSC [43] have perceptibly more prominent coherence peaks than the prediction, but otherwise the general course of the test results is in fair agreement with the mean field theory for doping not too far from optimal, and in excellent agreement as far as the unique features of the spectra are concerned: (i) the "hump and dip" occurring primarily on the hole side, at energies related to the gap and the doping percentage; (ii) their absence on the electron side; and (iii) the symmetry of the singularity at the gap energy. The asymmetry is incompatible with any perturbation method starting from weak coupling (as, for example spin fluctuation theory, or any phonon-based theory) and shows that the system must be described as a doped Mott insulator.

Case (iii) presents the underdoped case, in which it is expected a region of fluctuating "preformed pairs" between T_c and T^* that is the pseudogap is qualitatively predicted (see Fig. 2.6). The RVB state is initially an insulator on two causes: (i) at weak kinetic energy (that is, small effective t and domination of J), the spin-charge locking mechanism [40] does not work and the pairs are effectively neutral (ii) there is a commensurability energy which holds the structure in register with the crystal lattice (that is, the nodes are pinned at the $\pi/2$, $\pi/2$ points [1830]). As we add holes, the RVB structure does not change and provides the major proportion of the pseudoparticle self-energy. The hole excitations on the nodal lines will feel no or a small gap and show the putative Fermi surface for the ordinary kinetics energy, and such excitations form hole pockets. True superconductivity, when it develops, is confined at first to the pocket-arcs alone. This correlates with all the known experimental facts, including the "Fermi arc phenomenon" [811] and the mysterious simultaneous existence of strong Dirac nodes and hole pockets [1435]. Then, the correct approach to this region of the phase diagram is based in terms of a "Hidden RVB", as for the overdoped case it is the "Hidden Fermi Liquid".

The transport studies of the cuprate superconductors, carried out by Ong et al. [1774], discovered an extensive region of the p–T phase diagram in which these studies gave unequivocal evidence of quantized vorticity above the superconductivity temperature T_c. This discovery has been based on measurements of the Nernst effect and non-linear diamagnetism [1013, 1014]. The discovered equilibrium effect can be shown to be equivalent to the Nernst measurement if and only if the former is due to vortex motion. The region in which this occurs is shown for two sets of superconductive compounds in Fig. 2.7. The facts that these phenomena occur over a finite, in fact, extensive, region of phase space, and that one manifestation is a non-analyticity of an equilibrium property, argue that this is not critical fluctuations but a distinct new phase of matter. It is supported by models for T_c such as the two-dimensional Kosterlitz–Thouless one and XY model.

In the phase space region, discovered by Ong with co-authors, the electrons are apparently to be fairly strongly paired, superconductivity having been destroyed only by phase fluctuations of the order parameter, as demonstrated in [1470].

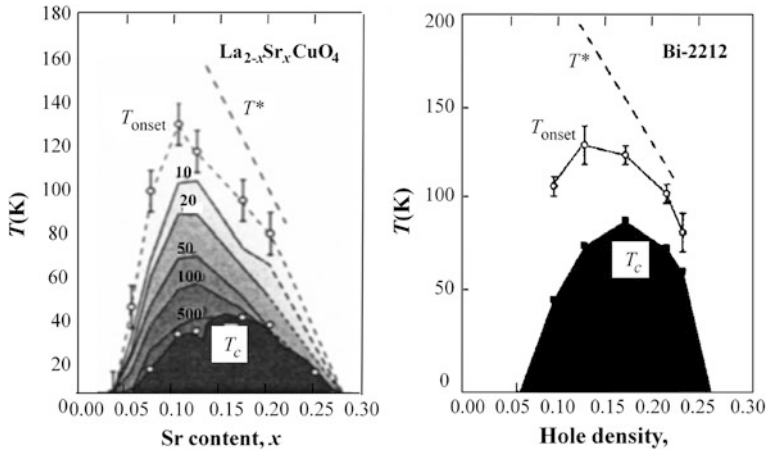

Fig. 2.7 The region of fluctuating phase ("vortex fluid") in which a vortex Nernst effect is measurable in two compounds with a range of doping [43]

Therefore, it is reasonable to think on the currents as being predominantly carried by paired electrons, i. e. bosons. If there is finite local pair amplitude above T_c, the pair wave function will have a time- and space-varying phase Φ and the pair current will be proportional to $\nabla\Phi$ and conserved. If so, Φ will be completely determined by a network of vortex lines—in three-dimensional case mostly vortex loops. Thus, it is appropriate to describe this phase as a "vortex liquid" [41, 42].

2.2.3 Influence of High Pressure on Superconductivity

In difference of majority superconductors, for which the critical temperature of superconductive transition T_c decreases with rise of pressure, in HTSC T_c increases usually. Studies of one-axis pressure witness that this increase in main degree is caused by decreasing a square, A, of CuO_2 planes ($T_c \propto A^{-2}$), but no distance between them. These results support theoretical models, which attribute superconductivity, in first order to intra-plane coupling interactions. Hence, the future experiments must state dependences on hydrostatic and one-axis pressure of the main parameters, namely: T_c, superconductive gap, pseudogap, carrier concentration and exchange interaction in all range of doping.

First studies of influence high pressures on superconductors have been carried out in 1925 by Sizoo and Onnes [1579], which discovered that for Sn and In, also as majority superconductors T_c decreased with growth of pressure. As it became to be clear afterwards, an explanation that diminishing was connected with the isotope effect. It is not be accidental, that many scientists apply the high-pressure techniques as important diagnostic instrument. It is defined that what the

experiments with using a high pressure could ensure valuable information for study superconductors with higher values of T_c.

In difference of magnetic materials, tremendous technological importance of which is caused by that, what their magnetism is stable to temperatures, which are far higher of usual ones, the material cannot become to be superconductive until not cooled at least on 160 K lower than above-mentioned temperatures. It is a very complex and elaborated process for long-length specimens, therefore most aim of superconductivity studies oriented on technological applications is creation materials with room temperature of superconductive transition.

One of the ways to understand ability of new superconductor to attain higher value of T_c is definition of dependence of T_c on chemical composition and/or pressure p. The great value of $|dT_c/dp|$ allows one to hope on possibility of attainment of the higher values of T_c. For example, successive application this strategy in experiments with high pressure on cuprate $La_{2-x}Ba_xCuO_4$ (La-214) has allowed Wu et al. [1810] to substitute La^{3+} cation by smaller Y^{3+} cation at high values of dT_c/dp (+8 K/GPa) and discover known superconductive compound $YBa_2Cu_3O_{7-\delta}$ (Y-123) with T_c, exceeding the liquid nitrogen temperature ($\sim$77 K). Another example is connected with oxide $La_{2-x}Sr_xCuO_4$, for which as it has been stated by Gugenberger et al. [589], T_c increases at the compression of material along one direction, at the same time decreasing at the compression along other direction. This fact has been used by Locquet et al. [1042], which created proper deformations in thin films of this oxide during their epitaxial growth on substrate and due to increased in two times the value of T_c from 25 up to 49 K. Finally, Klehe et al. [885] observed increase of T_c in conditions of high pressure applied to samples of $HgBa_2Ca_2Cu_3O_8$ (Hg-1223) that allowed to Gao et al. [515] to increase T_c for this superconductor from 134 K upon to $\sim$160 K. Moreover, Ashcroft [63] stated that elementary hydrogen could become room-temperature superconductor under very high pressure.

The experiments with high pressure contribute in superconductivity in some directions:

(i) as it has been above noted dT_c/dp is the well indicator that what higher values of T_c could be possible for given superconductor at ordinary pressure owing to the chemical substitution or using the technique of epitaxial growth,
(ii) some superconductors could be synthesized with proper properties only in conditions of high pressure and high temperature,
(iii) many non-superconducting materials could become superconductive at enough high pressure: to existing 29 elementary superconductors at ordinary pressure (Be, Al, Ti, V, Zn, Ga, Zr, Nb, Mo, Tc, Ru, Rh, Cd, In, Sn, Hf, Ta, W, Re, Os, Ir, Hg, Tl, Pb, La, Th, Pa, U, Am) from Mendeleev Table of Chemical Elements are added 23 ones, which become to be superconductive at application of pressure (Li, B, O, Si, P, S, Ca, Sc, Fe, Ge, As, Se, Br, Sr, Y, Sb, Te, I, Cs, Ba, Bi, Ce и Lu),

(iv) main electronic and crystalline lattice properties of superconductor change at the decreasing temperature due to thermal compression of the crystalline lattice, then the high pressure directly can change the lattice parameters at any temperature and so it allows one to correct the effects of the thermal compression at ordinary pressure,
(v) determination of dependences of T_c and other superconductive properties on individual parameters of the crystalline lattice of single sample creates a quantitative test for theoretical models and give information on the coupling mechanism.

For instance, if HTSC is caused, in first order by interlayer couple, then it may be proposed arising strong change of T_c, if apply one-axial pressure along perpendicular direction to layers. However, all experiments with high pressure differ one of others. In the case of superconductivity, the dependence of T_c on pressure p could be defined by medium used for creation of pressure and other factors. For example, the curve $T_c(p)$ obtained by Thomasson et al. [1667] for Pb by using pressure in rigid medium of "methanol–ethanol" disposed significantly higher than corresponding curve obtained for the same pressure but in the medium of helium.

In ideal case, the tests would be either totally hydrostatical, or only one-axis. However, the totally hydrostatical tests are possible only in restricted range of change of the pressure and temperature, because all liquids harden under pressure, for instance liquid helium freezes at the pressure of 12 GPa in the conditions of room temperature. The solid helium is very soft therefore it supports only very weak shear stresses. The dense He is used in experiments with high pressure as a pressure medium. One of the practical way to define, are the test results to be sensitive to effects of shear stresses, consists in use of two different pressure media. Achievement of highest values of T_c demands careful optimization of proper electronic and structural (crystalline lattice) properties. This optimization is especially difficultly to be realized in elementary bodies. Here, maximal value T_c is restricted by temperature range of 9–20 K (for Nb under ordinary pressure and for Li, B, P, S, Ca, V, Y, Zr and La at the very high pressures).

It is not surprising, that the multi-atomic systems demonstrate higher values of T_c since their structural flexibility allows greater degree of optimization. Quasi-two-dimensional solids (for example, HTSC, oxypnictides and MgB_2) demonstrate most values of T_c. However, the superconductive curates show great structural and electronic complexity as in ordinary conditions as under high pressures. This fact initiates numerous attempts to attain main understanding physical mechanisms which are responsible for superconductive state. The experiments, presented by Schilling [1498], confirm a conclusion on that what sizes of CuO_2 planes in greater degree determine maximal value of T_c for given HTSC, than a distance between these planes. The CuO_2 planes are to be plane and quadratic but decreasing their surface leads to rising magnitude of T_c. Thus, following Wijngaarden et al. [1798], it may be noted that c-axis causes in main case a doping, at the same time a-axis defines intrinsic T_c. Hence, interior interactions in the CuO_2 planes are responsible

in first order for superconductive pairing. Therefore, everywhere intrinsic dependence of T_c on volume ($T_c \propto V^{-1.2}$) for almost optimally doped HTSC is caused by rather compression of the CuO_2 planes than decreasing distance between them. Intrinsic dependence of T_c on crystalline lattice parameter, a, inside the plane for one-, two- and three-layer superconductive Hg-compounds is determined in the form, respectively: $d\ln T_c/d\ln a = -4.1$, -4.8 and -5.0. Hence, it may be obtained approximate dependence: $T_c \propto a^{-\delta}$, where $\delta = 4.5 \pm 0.5$. This dependence implies that an optimal doping is approximately inversely proportional to the square of region A of the CuO_2 planes, $T_c \propto A^{-2}$. Similar result has been obtained for other optimally doped HTSC. This one of most valuable results obtained in experiments on HTSC subjected to high pressure. In actuality, this information could not be obtained another means. Besides information on superconductivity mechanism, this dependence states additional strategy for following increasing T_c.

Thus, additionally to above-mentioned five rules (i–v) for optimization of T_c, it should be added sixth one, namely: (vi) it is required a search of structures applying maximal compression of the CuO_2 planes without their buckling.

In according to above relationships, if apply a pressure to optimally doped sample of Hg-1223 and compress its size in plane approximately on 20 % without addition of defects or increasing number of charge carriers, then T_c should rise from 134 K up to 304 K that is attain room-temperature superconductivity. In general case, HTSC systems with the same number of the CuO_2 planes at optimal doping have different values of $T_c^{\max}$.

It is interesting to elucidate, is this difference due to change of the lattice parameter, a, that is fulfills the dependence $T_c^{\max} \propto a^{-4.5}$. However, as it has been shown by tests there is not this simple correlation. The one-layer superconductor with highest T_c (Hg-1201), which has $T_c^{\max} \approx 98$ K, possesses most parameter a, but the compound with least value of T_c ($La_{1.85}Sr_{0.15}CuO_4$), which has $T_c^{\max} \approx 36$ K, demonstrates the least magnitude of a. It is possible, that $La_{1.85}Sr_{0.15}CuO_4$ shows anomalous low value of T_c due to excessive compression of the CuO_2 plane leading to strong structural distortions and buckling inside the plane that is to the effects which as it is well known decrease T_c. The values of a for other cuprate HTSC systems differs only into limits of 1.4 %, that corresponds to ~ 5 GPa or change of T_c only on 7–8 K. The pressure level increasing from 1.4 upon 20 % is deserving, but difficultly attainable aim for material science scientists. Important remaining moment is proof that the above-mentioned dependence $T_c^{\max} \propto a^{-4.5}$ will lead to superconductive state of HTSC.

If suppose that two electrons couple into Cooper pair with help of electron–phonon, electron–electron, electron–magnon or anybody another effective interaction, V_{eff}, then the BCS theory carries out for weak interactions and $T_c \approx \langle\omega\rangle \exp\{-1/[V_{eff}N(E_f)]\}$, where $\langle\omega\rangle$ is the characteristic energy of intermediate bosons, $N(E_f)$ is the electron density of states, E_f is Fermi energy. Since, the both parameters V_{eff} and $N(E_f)$ are included in the expression for exponent then it should be supposed that their dependence on pressure is responsible for the

critical temperature, T_c. The measurements of spin sensitivity at high pressures carried out for $La_{1.85}Sr_{0.15}CuO_4$ [23] and for Y-123 [22], and also calculations of structure of the energetic levels in Hg-1223 [1573] have stated that changes of $N(E_f)$ under pressure were lesser on 0.2, 0.1 and 0.5 %/GPa, respectively. In the case of $La_{1.85}Sr_{0.15}CuO_4$, this change of $N(E_f)$ was small due to fast increasing T_c under pressure. In order to make a similar estimate for Y-123 and Hg-1223, where dT_c/dp is far lesser, it is necessary to significantly increase an accuracy of definition of $dN(E_f)/dp$.

The remaining issue is: why $V_{eff}N(E_f)$ increases with pressure growth with the speed that $T_c \propto a^{-4.5}$. To regret, one only this dependence $T_c(a)$ does not give enough information, allowing simple identification of the pairing interaction. Intrinsic dependence of critical temperature on pressure dT_c/dp, which changes into approximate bounds from +1 up to 2 K/GPa for ideal HTSC decreases easily into broad limits, observed for superconductive transit metals, for which it has been stated the electron–phonon coupling. Based on analysis of results obtained for HTSC by using tests with high pressure, it has been concluded [1239] that the electron–phonon coupling is a possible superconductive mechanism also for HTSC.

To regret, the analysis leading to the intrinsic dependence of $T_c \propto a^{-4.5}$ is satisfactory only for HTSC near of optimal doping level. This restriction is introduced to exclude dependence of parameter n (the number of holes into CuO_2 plane) on pressure. In order to state intrinsic dependence $T_c^{\text{int}}(p)$ for wide range of doping, it is necessary first to carry out independent definition of dn/dp into the whole of this range. In order to understand the mechanism of the pairing interaction by using investigations fulfilled with application of high pressures, it is required to combine estimates obtained for $T_c(p)$ due to action of hydrostatic and one-axis pressures with simultaneous measurements (preferably on the same crystal) other important properties of superconductive and normal states, namely: superconductive gap, pseudo-gap into zone of underdoping, energy of superconductive condensation, magnetic sensitivity, electric resistance, Hall effect, etc. Then, it has been studied Raman scattering at high pressures in antiferromagnetic La_2CuO_4 and stated, that super-exchange interaction J increased approximately as $J \propto a^6$ [59].

These studies after spreading on HTSC could be used for testing a viability of spin-fluctuation theories. The measurements of magnetic sensitivity in dependence on pressure at the elevated temperatures should ensure similar information on J (p). However, following studies on the La-214 system can lead to error conclusions because strong structural distortions and transitions, which are characteristic for this system, make quantitative analysis very complex. More real attempt is connected with these studies fulfilled on monocrystals of Hg- and Tl-superconductive families into the whole of range of the doping change. Especial attention should be given to the experiments with one-axis pressure, since they can possess necessary detail information.

2.2.4 Specific-Heat Anomaly at Temperature of Superconducting Transition in HTSC

Due to short coherence length in HTSC, the fluctuation effects in specific heat near transition temperature T_c at zero field which have observed in conventional low-temperature superconductors, to be also proper for HTSC. However, there is vagueness: are these fluctuations to be two- or three-dimensional and Gaussian or critical? For magneto-field measurements is also important an issue of applying set of the scaling relationships. Other fundamental moment connected with anomaly of heat capacity near T_c is change of anomaly shape in dependence on doping level. The experimental witnesses that what this change of the anomaly shape reflects alteration from the BCS-transition to one of the transition being a variant of the Bose–Einstein condensation, have been presented by Fisher et al. [483].The specific-heat anomaly at the transition temperature T_c is better found in YBCO and *RE*BCO compounds compared to other HTSC.

Ginzburg–Landau (GL) theory can well explain into framework of the mean field approximation the character of phase transition in superconductors satisfying the BCS-theory and predicts the transition behavior until the fluctuation effects are sufficiently small and can be described by Gaussian distribution. However, at the enough approximation of T to T_c, when the sample to be already in critical zone, in order to describe the fluctuations, the renormalization group theory is more available, which has been developed for description of phase transitions by Goldenfeld [540]. The temperature regions, in which two kinds of fluctuations expect, are compared in size with mean-field discontinuity $\Delta C_e(T_c)$, expressed in terms of the Ginzburg criterion [534] or lesser-known criterion of Brout [188]. Here, C_e is the contribution into specific heat of conductivity electrons. The both criteria could be expressed in terms of the normalized temperature $t = (T/T_c - 1)$. Due to these criteria the critical region of three-dimensional superconductor is situated into range $|t| < t_G = \{k_B/[\pi\Delta C_e(T_c)\xi^3]\}^2/32$, where $\xi = (\xi_a\xi_b\xi_c)^{1/3}$ is the GL coherence length of superconductive order parameter at $T = 0$. The parameter $\Delta C_e(T_c)$ is expressed in units of energy density, K^{-1}, k_B is Boltzmann constant.

The Gaussian fluctuations stated by Kapitulnik et al. [813] could be expressed into wider range $1 \gg t_B > |t| > t_G$, where $t_B \sim (t_G)^{1/2}$. The contribution of fluctuations into anomaly of specific heat near T_c, is determined by positive curvature of C_e/T lower of T_c and "tail" upper T_c. There is important witness that superconductivity in HTSC is characterized by a strong couple which increases $\Delta C_e(T_c)$, and also creates a positive curvature lower T_c. Therefore, the possibility of strong couple introduces further indefiniteness in addition to that which is associated with selection of the crystalline lattice contribution in analysis of specific heat near T_c. Strong dependence of both as t_B, as t_G on ξ make to be obvious that what the coherence length is defining factor without dependence on existence of the fluctuation effects. In the case of typical type-I superconductor, for example Sn with $\Delta C_e(T_c) \sim 1$ mJ/(cm^3 K) and $\xi \sim 2000$ Å, $t_G \sim 10^{-14}$ and $t_B \sim 10^{-7}$ [1203], the Brout criterion affirms that the contribution of the Gaussian fluctuations cannot

be observed without making measurements of specific heat into range of 1 μK or lesser near T_c. Therefore, it is not surprising that the specific-heat anomalies near T_c of conventional superconductor are well described by standard mean-field theory. On contrary, in the case of HTSC, for instance YBCO with $\Delta C_e(T_c) \sim 30$ mJ/(cm^3 K), $\xi \sim 10$ Å and $T_c \sim 90$ K, $t_G \sim 0.0015$ and $t_B \sim 0.04$ [1203]. In this case, the Ginzburg criterion and Brout criterion propose that the Gaussian fluctuations would take place into range of $\sim$5 K near T_c, at the same time the critical fluctuations would be into much more narrower range of $\sim$0.1 K near T_c.

The calculations [50, 753] have shown that for *s*-wave pairing, the contribution of the Gaussian fluctuations C_f into C_e at zero magnetic field could be written as $C_f^{\pm} = A^{\pm}[k_B/(16\pi\xi^d)]|t|^{-\alpha}$, where $\alpha = (4 - D)/2$, D is the system dimensionality, $A^+ = 2$ and $A^- = 2^{D/2}$ for $t > 0$ and $t < 0$, respectively. The more earlier measurements of C_f [752] corresponded to $\alpha = ½$, as it was expected for three-dimensional systems, but in this moment there have not been obtained values of A^+ and A^- or their ratio A^+/A^-. Then, it has been shown that in critical region, C_f may be presented as $C_f^{\pm} = (A^{\pm}/\alpha)|t|^{-\alpha}$, where the "critical exponent" α and factors $A^{\pm}$ are constants, depending on "universality class" (three-dimensional *XY*, Ising, etc.) [1506]. By this, the value of α is to be near but no equal to zero. For very small α, the term $|t|^{-\alpha}$ could be replaced by $(1 - \alpha \ln|t|)$.

While the Ginzburg and Brout criteria are useful rules, but do not allow one to differ the regions of the Gaussian and critical fluctuations. For example, it has been supposed for type-II superconductors, that the bounds of critical region exceed the value of t_G in difference on that how this was defined above [480]. Moreover, there is divergence with nature of crossover from the Gaussian to critical fluctuations. Therefore, due to the pointed discrepancies as with definition of wide of the critical region, as form of the fluctuation term in each region of the crossover, it is useful to carry out a comparison with test data. Different research groups (see [801]) have shown that for optimally doped YBCO and DyBCO monocrystals the specific heat is well predicted by using three-dimensional *XY*-model [540, 1506], which well describes λ-transition of liquid ^{4}He [1026].

In the existence of field, the measurement results of optimally doped *RE*BCO in the case of critical representation coincide better with three-dimensional *XY*-model, compared to the Gaussian case. As it has been shown [993], the field and temperature dependence of C_f could be presented as $C_f = C_0 - B^{\alpha/2\nu} f(x)$, where $C_0 = 0$ for $t > 0$ and is to be constant for $t < 0$, $x = t/B^{1/2\nu}$, α is the heat capacity exponent, and ν is the coherence length exponent, for example $\xi(t) = \xi/t^{\nu}$. In the fluctuation equation arises scaled temperature x, but no normalized temperature t as before. The simplified form of the equation for fluctuation, as it has been shown in [1470] could be written as $[C(0, T) - C(B, T)]B^{\alpha/2\nu} = f(x)$, where $\nu = 0.669$ in the case of three-dimensional *XY*-model, and $\alpha = -0.013$ is the test value obtained for ^{4}He. Advantage of the simplified equation consists in that what it allows one to predict the scaling without assumptions stated for crystalline lattice specific heat C_{lat}, excepting that what it independents on magnetic field B. In practice, because of indefiniteness of estimate of the critical temperature T_c,

the authors prefer to define it on the base of known values rather than based on measurements of $C(0, T)$.

The satisfactory of the three-dimensional *XY*-model for description of critical behavior of the optimally doped *RE*BCO has been stated [801]. Some authors tested predictions of the three-dimensional *XY*-scaling studying as derivatives of C change in dependence on field and temperature. Additionally, there have been studied predictions of scaling with aim to apply them to field dependence of magnetization. Moreover, it has been verified applicability another approach to scaling, namely the lowest Landau level (LLL-scaling) [1361]. While, there is discrepancy in opinions relatively most acceptable range of magnetic field B change for given scaling procedure, however, if it is suggested that the upper critical field $B_{c2}(T)$ changes as $|t|^{4/3}$, but not as $|t|$, then the both models (three-dimensional *XY* and LLL) ensure satisfactory description the specific heat and magnetization under magnetic fields from 1 up to 16 T.

The anomaly height of specific heat in optimally and weakly overdoped *RE*BCO could be of order 3–4 % from C. In the case of underdoped superconductive *RE*BCO, this height in general case is lower, at the same time it seldom exceeds 1.5 % from C in La-, Tl- Bi-, and Hg-HTSC. The measurements fulfilled on Pb-stabilized Bi-2212 [1266] and on Bi-2212 [1507] agreed with two-dimensional (but no three-dimensional) Gaussian fluctuations, since it has been stated, that C_f changed as $|t|^{-1}$, but not as $|t|^{-1/2}$. Existing experimental data for Tl-2201, Hg-1201 and Hg-1223 demonstrate the specific-heat anomaly which is similar to Bi-2212.

2.2.5 Coherence Length and HTSC Anisotropy

Despite the fact that there is no definite theory to explain high critical temperatures of HTSC, their magnetic and superconducting properties can be well described (as it has been noted above) into framework of the classical BCS/Ginzburg–Landau theory. They demonstrate a set of properties that are similar to conventional low-temperature superconductors. In particular, superconductivity in cuprates occurs due to coupling of electrons. Moreover, there is energy gap in a spectrum of electron excitations that is caused by electron coupling. Non-monotonous dependence $T_c(p)$ (see Fig. 2.3) is similar to non-monotonous behavior $T_c(p)$ of superconducting semiconductors. Finally, isotope effect also exists in cuprates, while it is directly found by the concentration of holes [1201].

The main difference from conventional superconductors is caused by intrinsic material properties, for example, the extremely short coherence length ξ (in conventional superconductors $\xi = 400 - 10^4$ Å). Short coherence length is a consequence of the big energy gap and the small Fermi velocity. Due to the extremely short coherence length, even a grain boundary can be sufficient to suppress superconductivity in cuprates. In particular, the grain boundaries can be

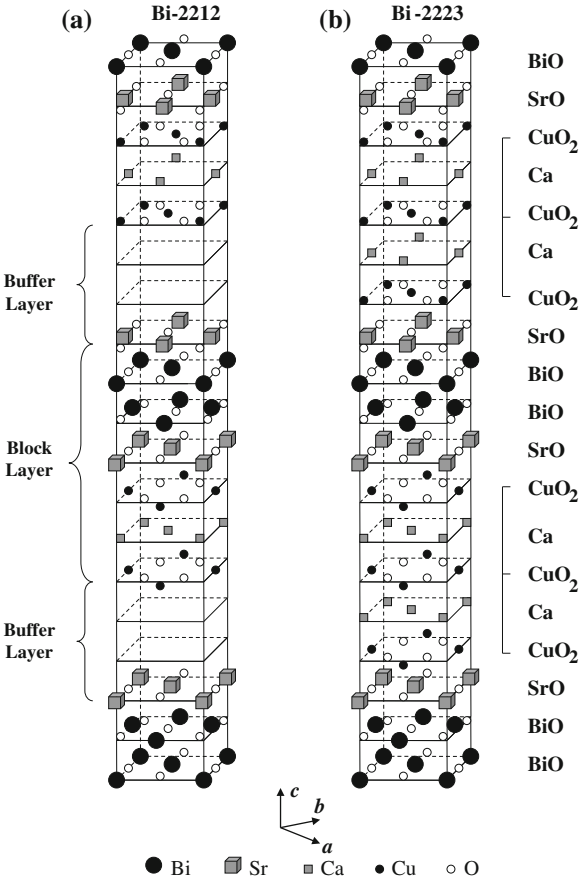

Fig. 2.8 Crystalline structures of Bi-2212 (**a**) and Bi-2223 (**b**). The layered structure of Bi-2212 can be divided into block layers and buffer layers for intercalation of additional Ca/CuO_2 plane, forming Bi-2223. The height shown of buffer layers in the structure of Bi-2212 is expanded to compare with real one for clearness of comparison of both structures [224]. Below, the principal axes *a*, *b* and *c* are shown

used to fabricate devices of Josephson type (in the form of epitaxial films on bi-crystalline substrates), based on the existence of weak links.

The second important property of high-temperature superconductors is their huge anisotropy caused by the layered crystalline perovskite structure.[3] For example, $Bi_2Sr_2CaCu_2O_8$ (Bi-2212) crystal, presented in Fig. 2.8a, consists of the sequence of CuO_2 planes, alternating with other oxide layers. The basic block is the CuO_2 double layer (intercalated by Ca). These blocks are separated by four oxide layers namely two SrO and two BiO ones. In Fig. 2.8b, a process of intercalation of the additional Ca/CuO_2 plane is present to form $Bi_2Sr_2Ca_2Cu_3O_{10}$ (Bi-2223) crystal.

Due to two-dimensional structure of cuprates, the coherence length depends on the crystallographic direction, namely along *c*-axis the value ξ_c is far lesser than in *ab*-plane (ξ_{ab}). In the different hole-doped cuprates, $\xi_{ab} = 10$–35 Å, at the same

[3] Crystalline structures of some HTSCs are present in Appendix A.

Table 2.1 Characteristics of optimally doped cuprates [1201]

Material	T_c (K)	ξ_{ab} (Å)	ξ_c (Å)	λ_{ab} (Å)	λ_c (Å)	$B_{c2\parallel}$ (T)	$B_{c2\perp}$ (T)
NCCO	24	70–80	~15	1200	260000	7	–
LSCO	38	33	2.5	2000	20000	80	15
YBCO	93	13	2	1450	6000	150	40
Bi-2212	95	15	1	1800	7000	120	30
Bi-2223	110	13	1	2000	10000	250	30
Tl-1224	128	14	1	1500	–	160	–
Hg-1223	135	13	2	1770	30000	190	–

time, $\xi_c = 1$–5 Å. As a rule, the coherence length of cuprates with low critical temperature is longer than in cuprates with high T_c (see Table 2.1). In electron-doped NCCO, the coherence length is in some times longer than in other hole-doped cuprates. Small values of ξ_c mean that transport along the c-axis is not coherent, even in the superconducting state. For example, $\xi_c \sim 1$ Å in Bi-2212 that is in some times shorter compared to the distance between layers.

Two critical fields $H_{c2\parallel}$ and $H_{c2\perp}$, directed parallel and perpendicular to the basic ab-plane, respectively, correspond to two principle axes (in ab-plane and along c-axis). The notation is as follows. The upper critical field perpendicular to the ab-plane, $H_{c2\perp}$, is determined by vortices (with magnetic flux Φ_0) whose screening currents flow parallel to this plane. Then, for the dependence between critical field and coherence length, we have the following equation [1502]:

$$H_{c2\perp} = \frac{\Phi_0}{2\pi\xi_{ab}^2}. \tag{2.2}$$

The indices ab or c of parameters λ and ξ show the directions of the screening currents.

Due to the high-temperature superconductors possess the layered crystal structure superconductivity in HTSC is confined to the CuO_2 planes. They are separated from neighboring planes by weakly superconducting, normal or even insulating regions of the crystal. Three-dimensional phase coherence is provided by the Josephson currents, which flow between above planes. If we assume a homogeneous order parameter and use description of anisotropy in the framework of the Ginzburg–Landau theory, then for parameter $H_{c2\parallel}$ we have

$$H_{c2||} = \frac{\Phi_0}{2\pi\xi_{ab}\xi_c}; \tag{2.3}$$

then the anisotropy ratio is

$$\frac{H_{c2||}}{H_{c2\perp}} = \frac{\xi_{ab}}{\xi_c}. \tag{2.4}$$

In the case of weakly anisotropic material, such as $YBa_2Cu_3O_{7-x}$, this representation is sufficient. However, for anisotropic material, such as $Bi_2Sr_2CaCu_2O_8$, the value of ξ_c then would be of the order of 0.1 nm, that is approaching atomic

scales. In any case, this contradicts the assumption of a homogeneous order parameter. In cuprates, low critical fields $B_{c1\|}$ and $B_{c1\perp}$ are very small. For example, in YBCO $B_{c1\|} \sim 2 \times 10^{-2}$ T and $B_{c1\perp} \sim 5 \times 10^{-2}$ T. It is interesting that anisotropy of values B_{c1} has different sign than of B_{c2}, namely $B_{c2\perp} < B_{c2\|}$ and $B_{c1\perp} > B_{c1\|}$. In conventional superconductors, $B_{c2} \propto T_c^2$; at the same time, $B_{c2} \propto T_c^{\sqrt{2}}$ [1201] in cuprates with low T_c. The extreme anisotropy is also responsible for many particular effects associated with the flux line lattice in high-temperature superconductors.

2.2.6 Vortex Structure of HTSC and Magnetic Flux Pinning

The layered structure of the cuprate superconductors, with the superconductivity arising within the CuO_2 planes, causes the properties of a single vortex. The orientation of the CuO_2 planes is defined by the crystallographic *a*- and *b*-axes. The CuO_2 planes are coupled to each other by Josephson junctions. Lawrence and Doniach proposed the phenomenological model for this layered structure [992]. The Lawrence–Doniach theory contains the anisotropic Ginzburg–Landau and London theories as limiting cases, when the coherence length ξ_c in *c*-direction exceeds the distance between layers *s*. In this limit, the anisotropy may be considered in terms of the reciprocal mass tensor with the principal values $1/m_{ab}$, $1/m_{ab}$ and $1/m_c$. Here m_{ab} and m_c are the effective masses of Cooper pairs, moving into *ab* plane and along the *c*-axis, respectively. If the interlayer coupling is weak, then we have $m_{ab} \ll m_c$. Into framework of the anisotropic Ginzburg–Landau limit, the extended relations (2.4) may be obtained:

$$\left(\frac{m_c}{m_{ab}}\right)^{1/2} = \frac{\lambda_c}{\lambda_{ab}} = \frac{\xi_{ab}}{\xi_c} = \frac{H_{c2\|}}{H_{c2\perp}} = \frac{H_{c1\perp}}{H_{c1\|}}. \tag{2.5}$$

If magnetic field is oriented along the *c*-axis, the flux lines reduce to stacks of two-dimensional point vortices or pancake vortices. A detailed modeling of the layered cuprate superconductor in terms of a stack of thin superconducting films into framework of the Lawrence–Doniach theory has been carried out [295, 481]. Energetically, the perfect stacking of the pancake vortices along *c*-axis is favorable, than a more disordered structure. At the same time, compared to a continuous flux line, as it exists in the conventional superconductors, a stack of the pancake vortices has additional degrees of freedom for thermal excitations. As an example, we consider the displacement of a single pancake vortex, presented in Fig. 2.9. This displacement is equivalent to the excitation of a vortex–antivortex pair (Kosterlitz–Thouless transition), possessing the interaction energy [725]: $U(r) = \varphi_0^2/(\mu_0 r)$, where φ_0 is the quantum of magnetic flux, μ_0 is the vacuum permeability and r the distance between the vortex and antivortex. For two-dimensional screening length, Λ, we have the binding energy, $U(r) \approx \varphi_0^2/(\mu_0 \Lambda)$.

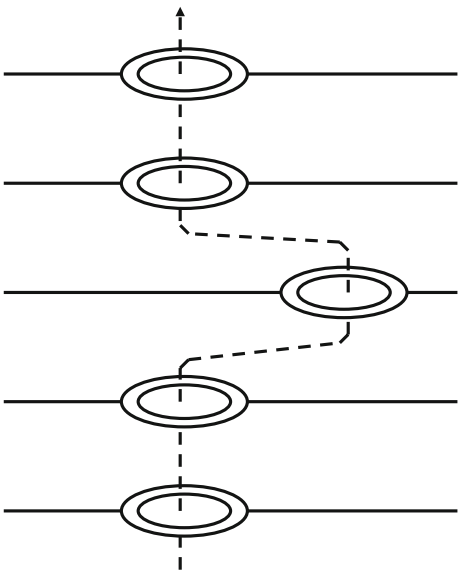

Fig. 2.9 Displacement of a single pancake vortex

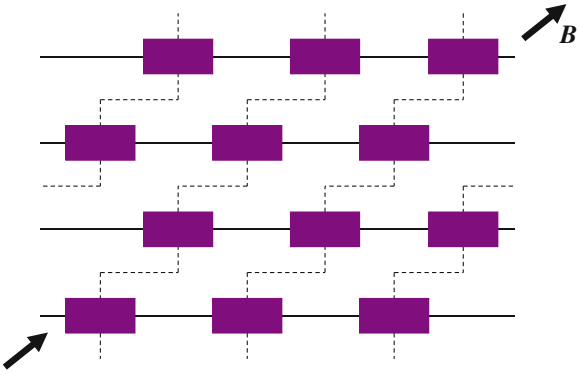

Fig. 2.10 Pancake vortices (*gray rectangles*) coupled by Josephson strings (*horizontal dashed lines*)

By interpreting the displacement of a single pancake vortex as an evaporation process, the evaporation temperature, T_D, has form [295]:

$$T_D \approx \frac{1}{k_B}\frac{\varphi_0^2}{\mu_0 \Lambda}. \tag{2.6}$$

When an external field is nearly parallel to the *ab*-plane, the vortex core preferably runs between the CuO_2 layers. When the coupling between layers is weak, vortex lines along the *ab*-plane are referred to as Josephson vortices or strings. For any magnetic field direction not parallel to the *ab*-plane, the pancake vortices existing in the CuO_2 planes are coupled by such Josephson strings, as shown in Fig. 2.10.

Investigation of the temperature and magnetic field dependence of the magnetization in the powder samples of Ba–La–Cu–O [1206] discovered *an irreversibility line* in the *H–T* phase space (*H* is the magnetic field, *T* is the temperature). Above this line, the magnetization is perfectly reversible with no detectable magnetic flux pinning. However, below this line the hysteresis of *magnetization* arises, and the equilibrium vortex distribution can no longer be established due to *the magnetic flux pinning*. Soon after this discovery, a similar line was found in YBCO single crystal [1836]. Due to these and similar observations, the concept of "vortex matter" may be stated, taking *a liquid, glassy or crystalline* state in the phase diagram. These features have important influence on the transport processes associated with vortex motion. The vortex lattice, originally proposed by Abrikosov [4], consisted of a regular configuration of the magnetic flux lines in the form of a triangle (hexagonal) or square lattice that minimized their interaction energy (see Fig. 2.2). In HTSC, thermal energies are large enough to melt the Abrikosov vortex lattice (at $H = H_m < H_{c2}$), forming a vortex liquid over a large part of the phase diagram. In addition to the high temperatures, there is the structure of magnetic flux lines, consisting of individual, more or less strongly coupled pancake vortices, which promote this *melting transition*. In order to avoid energy dissipation at existence of transport current, each vortex should be fixed at pinning center. In this case, linear and plane defects are most effective. Increasing the number of defects is capable of moving the line $H_m(T)$ at phase diagram into a region of greater values of H and T. There is a universal field, H_1, such that $H_1(T) < H_m(T) < H_{c2}(T)$, at which thermodynamic fluctuations of order parameter lead to tearing of vortices from lengthy pinning centers [478]. This field presents upper boundary of the irreversibility field, $H_{irr}(T)$, at which the dissipation begins.

The simplest theoretical description of a melting transition is based on the Lindemann criterion, according to which a crystal melts if the thermal fluctuations $\langle u^2 \rangle^{1/2} = c_L a$ of the atomic positions are of the order of the lattice constant a. The Lindemann parameter $c_L \approx 0.1$–0.2 depends only slightly on the specific material. This approach has been used to determine the melting transition of vortex lattices. In particular, expressions for the melting temperature in the two- and three-dimensional cases have been derived [146, 170, 172, 482, 1681]. A schematic phase diagram for melting of the solid vortex lattice for three-dimensional material such as YBCO with field applied parallel to the *c*-axis is shown in Fig. 2.11.

The various parts of the vortex phase diagram are caused by competition of four energies, namely thermal, vortex interaction, vortex coupling between layers and pinning. The thermal energy pushes the vortex structure towards the liquid state, the interaction energy favors lattice state, the coupling energy tends to align the pancake vortices in the form of linear stacks and the pinning energy generates disorder. An interaction of these energies, whose relative contributions vary strongly with magnetic field and temperature, results in the complex phase behavior defined by the vortex matter. Then, the irreversibility line may be interpreted as the melting line, above which the state of the vortex liquid is

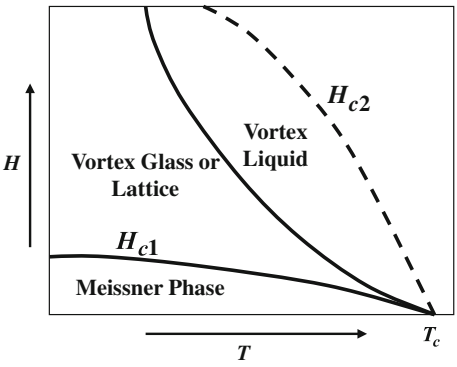

Fig. 2.11 Schematic phase diagram for a three-dimensional material such as YBCO [725]

attained, and below which there is the state of the vortex glass or vortex lattice. The vortex glass state is connected with magnetic flux pinning in the sample, disrupting any vortex motion. The first clear evidence for vortex lattice melting has been obtained from transport measurements (electrical resistance) for de-twinned single crystals of YBCO with $\boldsymbol{H}$ parallel to the c-axis. At a well-defined freezing temperature of the magnetic flux T_m, which depends on the magnetic field, a sudden drop to zero of the resistivity was observed, defining the onset of strong pinning in the vortex solid. The sharp drop of the resistivity at T_m demonstrates *a first-order freezing transition* [312]. *The first order vortex-lattice melting transition* has been observed in thermodynamic measurements, using a high-quality single crystal of BSCCO with $\boldsymbol{H}$, again parallel to the c-axis [1865]. Review, devoted to vortex matter and its melting transition, has been presented in [313].

Early investigations of transport processes in HTSC demonstrated the power dependence of volt–ampere I–V characteristic (I is the current, V is the voltage) [904, 1863] that in the following has been selected as a criterion for the freezing transition into limit of the superconducting vortex glass structure. In another interpretation, a distribution of the activation energy is used for this [575].

Weakening of flux pinning by melting of the vortex lattice is expected only when there are many more flux lines to compare with existing pinning centers. At the same time, in the opposite case, softening of the vortex lattice often leads to stronger pinning than in a rigid vortex lattice. This is explained by the concept that the atomic-scale defects (also as oxygen vacancies) can act as pinning centers for HTSC (the case is often realized in practice). Therefore, melting of vortex matter does not necessarily result in a reduction of pinning. Because of the complexity of this question, there is no simple answer (I see reviews [171, 172]). Flux pinning is caused by spatial heterogeneity of the superconducting material, leading to local depression in the Gibbs free energy density of the magnetic flux structure. Due to the short coherence length in HTSC, heterogeneities, even on an atomic scale, can act as pinning centers. As these important examples, we note deviations from stoichiometry, oxygen vacancies in the CuO_2 planes, and twin boundaries. The separation of a flux line into individual pancake vortices also promotes pinning caused by atomic size defects.

An original discussion of magnetic flux pinning caused by atomic defects in the superconducting CuO_2 planes (in this case by oxygen vacancies) has been carried out in [847, 1734]. By this, the elementary pinning interaction of vortices with the oxygen vacancies was calculated, and the vacancy concentration was related to the critical current density. The various structure defects in HTSC, acting as *pinning centers*, were considered in review [1807], but a detailed research of pinning effect on magnetic relaxation has been carried out in paper [1837]. An advance in solution of the problem of the statistical summation of pinning forces has been attained into framework of the Larkin–Ovchinnikov theory of collective pinning [984]. In this theory, the elastic deformation of the vortex lattice in the presence of a random spatial distribution of pinning centers plays a central role, but the increase of the elastic energy is balanced by the energy gained by passing the flux lines through favorable pinning sites. A discussion of corresponding physical basis is represented in monograph [1681]. We shall return to the discussion of the flux pinning problem in other chapters of our book.

2.2.7 Interactions of Vortices with Pinning Centers

As has been noted, for the attainment of high density of the critical current, it is necessary that microstructure of superconductor retained vortex lines of magnetic flux on the moving, caused by the Lorentz forces. It is reached only by pinning of vortices on the microstructure heterogeneities (or defects). However, no any defect can effectively interact with vortex lines. For example, in conventional superconductors, vacancies, individual atoms of secondary phases or other similar tiny defects are not effective pinning centers due to obvious causes: as a rule, a specific size of vortex (coherence length) is far greater than atomic size, that is, proper size of this defect. Therefore, vortex line simply "does not notice" them. On the contrary, the structure defects with size of $\sim\xi$ and greater become effective ones in this sense, and they can cause high density of critical current.

However, in the case of HTSC there is another situation. Here, the coherence length is extremely short, and point defects have sizes commensurable with ξ. Therefore, consider in more detail a situation arisen on example of vortex interaction with a cavity in superconductor.

Consider an infinite superconductor, containing a defect in the form of a cylindrical cavity. How will a single vortex parallel to the cavity interact with it? Assume that the diameter of the cavity, d, satisfies the inequality $d > \xi(T)$. If the vortex is far away from the cavity, its normal core (of diameter $\sim 2\xi$) stores a positive energy (relative to the energy of the superconductor without the vortex), because the free energy of the normal state exceeds that of the superconducting state by $H_{cm}^2/8\pi$ (per unit volume). Then, the energy of the normal core (per unit length) is

$$\frac{H_{cm}^2}{8\pi}\pi\xi^2. \tag{2.7}$$

On the other hand, if the vortex is trapped by the cavity, that is, passes through its interior, then it does not have a normal core and, accordingly, the energy of the system is reduced by the amount of (2.7). This means that the vortex is attracted to the cavity. The interaction force per unit length, f_p, can be found easily, if we recall that the energy changes by the value of (2.7), when the vortex changes its position near the edge of the cavity by $\sim\xi$

$$f_p \approx H_{cm}^2\xi^2/8. \tag{2.8}$$

For a spherical cavity of diameter d, the interaction force f_{pd} caused by the vortex can be obtained from (2.8) in the form

$$f_{pd} \approx H_{cm}^2\xi d/8 \tag{2.9}$$

To get an idea of how large this force is, let us find the current (j) that must be applied in the direction perpendicular to the vortex in order to produce the Lorentz force $f_L > f_{pd}$. It is known that the Lorentz force per unit length of a vortex is $j\Phi_0/c$ (Φ_0 is the magnetic flux of the vortex, c is the speed of light in vacuum) [1502]. Then, the force applied to the part of the vortex which actually interacts with the defect is $j\Phi_0 d/c$. By equating this to f_{pd}, from (2.9), we obtain

$$j = \frac{cH_{cm}^2}{8\Phi_0}\xi. \tag{2.10}$$

Furthermore, since $H_{cm} = \Phi_0/(2\sqrt{2}\pi\lambda\xi)$ [1502], then from (2.10) we obtain

$$j = \frac{cH_{cm}}{16\sqrt{2}\pi\lambda}. \tag{2.11}$$

It may be shown that j in the last expression is of the same order of magnitude as the Cooper pair-breaking current [1502]. Thus, in order to tear the vortex off a spherical void, it is necessary to apply the maximum possible current for a given superconductor.

The above discussion is also applied to a superconductor, containing tiny dielectric inclusions. It also remains valid (at least by the order of magnitude) for normal metal inclusions, provided the size of the inclusions is larger than ξ. The restriction is caused by the *proximity effect,*[4] which is essential only at distances of the order of the coherence length ξ from the interface. Therefore, the various types

[4] If thin layer of a superconductor is brought in contact with layer of a normal metal, then pairs of electrons with summary zero impulse, formed in the superconductor will stretch on both layers. Proximity effect depends on the interface nature and the relative thickness of both layers.

of inclusions present effective pinning centers in superconductors. This property is widely used in technical applications, when large critical currents and magnetic fields act.

As effective pining centers in superconductors we also note dislocations, dislocation walls, grain boundaries and interfaces between different superconductors. The above analysis of vortex-defect interactions forms the basis for interpretation of effects caused by the so-called *columnar defects* [1173], produced in high-temperature superconductors by irradiation. In this case, the normal cylindrical amorphous regions are formed in the superconductor. The nuclear tracks represent themselves as cylindrical regions with diameter being only 5–10 nm, that is, of the order of the coherence length ξ. As we have just seen, cavities of such sizes are effective pinning centers. This is one of the very few possibilities for producing artificial defects of sizes comparable with the coherence length in HTSC. In given materials, the coherence length is so short that any metallurgical methods used to produce pinning centers, such as precipitates or grain boundaries, have small effect, due to the disproportional size of defects, or not applicable at all, due to the brittleness of the material.

Each defect is capable of trapping approximately one vortex. Hence the optimum pinning efficiency can be expected at magnetic fields, for which the vortex lattice period is less than the average distance between the amorphous tracks. When the Lorentz force[5] caused by the applied field becomes greater than an interaction force with defect or heterogeneity, then a displacement of vortex flux leads to energy dissipation and initiation of finite electrical resistance. This state of vortex structure is called the *resistive state*.

As may be expected, vortex moving caused by the Lorentz force and corresponding resistance to magnetic flux strongly depend on three unique properties of HTSC, namely high critical temperature, small coherence length and layered anisotropic structure. Combining the above features strongly facilitates vortex moving and destroys superconductivity. Due to this, the *resistive transition* essentially expands in magnetic field. This is one from causes, stimulating tremendous efforts of material scientists directed to change of the HTSC manufacture technology with aim to decrease the vortex moving, making more active the magnetic flux pinning. Obviously, this problem will be complicated with the discovery of superconductors, possessing even greater temperatures of transition into superconducting state.[6] Composition features and modern manufacture techniques for basic HTSC systems will be considered in Chap. 3.

[5] In general case, the Lorentz forces can be initiated as transport current, as screening currents caused by sample magnetization.

[6] Nevertheless, it is not obligatory that superconductors with transition temperatures near to room temperature will possess oxide structure.

2.2.8 Future Studies of Vortex State

Study of vortices in superfluid directly connected with the problems its turbulence which due to Feynman is the state with disorder sequence of quantified vortices. Since the vortex structure is topologically stable object in superfluid and only idealization into framework of classic liquid, then the turbulence of the superfluid could help to attain a new understanding turbulence in general case. Moreover, this could help to investigate mutual links between superconductivity and ferro-(antiferro-) magnetism. The interests of study of the vortex state are not restricted only by study of vortex structures for several single vortices, but also expanded on investigation collective effects of great number of the vortices and vortex lattices, and also on their interaction with material structure and defects with account of the superconductor topology and geometry.

The studies of the Ginzburg–Landau (GL) equations for fullerene-like structures could lead to novel understanding on vortex state in Josephson junction arrays. Moreover, interaction of vortices with other objects, for instance vortex structure of the Bose–Einstein condensate in optical traps and their interaction with lasers are also interesting objects for future studies.

Note the following perspective mathematical directions of future investigations:

(1) *Vortex creep*. Since, the temperature fluctuations cause motion, for example vortex vibration, then this, in one's turn, leads to arising electric resistance, which can tear vortices from their flux pinning centers. While definite results of computer simulation of these processes have been obtained, the strict mathematical theory remains to be restricted. These problems are related to study of vortex glass and liquid states, and also critical fields and transition temperatures between glassy state (when vortices are to be stationary or pinned) and liquid one (when moving vortices possess definite electric resistance).
(2) *Critical currents*. Great applied currents or magnetic fields also fracture holding pinning forces and cause vortex motion introducing electric resistance. Preliminary studies of vortex states in presence of external fields have been fulfilled as well as computer simulation of movement of spatially-periodic vortices. However, complete mathematical description of these processes is to be very approximate.
(3) *Three-dimensional vortex structure*. Movement, entanglement, orientation, pinning, etc. of vortex lines in three-dimensional statement, as well as collective properties of great number of the vortices, their properties of elastic and plastic states require fulfillment of corresponding mathematical studies.

As problems connected with technical applications of superconductivity, note optimal design of composite superconductors, in particular definition most better distribution of pinning centers which are capable to support high currents, and also control the movement ways and speeds of the vortex lines that could be important at designing superconductive devices. From viewpoint of computational processes

numerous questions remain which are related to strong analysis of computer algorithms, in particular to schemes of partition on time of non-linear GL equations depending on time. In the case of the vortex density models, the numerical analysis is still restricted in a whole by two-dimensional examples. Therefore, generalization to three-dimensional models is to be required and perspective stage of the following studies. With practical viewpoint, the computer simulation of enough great number of vortices based on the GL model is very interesting. However, it is still accompanied by great computation difficulties, in particular owing to insufficiently studied effect of the vortex quantization.

Speaking more concretely, for square sample with n internal vortices, the phase angle of complex order parameter will demonstrate change on value of $2n\pi$ near the specimen boundary. If m points are necessary to obtain numerical solution for this single period of phase change, then $mn/4$ points required for each side of the square specimen. Thus, the computational network will demand $m^2n^2/16$ nodes. In the case of great values of n and even moderate values of m this can lead to very significant computational difficulties even in two-dimensional statement of the problem no speaking on three-dimensional case.

It is natural that the adaptive schemes and parallel calculations could significantly decrease the computational difficulties. However, in the case of densely-located vortices, decreasing the network scale could be required practically everywhere, and effectiveness of these schemes will far lesser. In particular note that it is not enough to decrease the network only near the vortex cores, because correct study of phase change is also to be very important. Enough exact definition of high phase oscillations for correct statement of effect of the topological quantization will accompanied by computational difficulties which similar, for instance to definition of high-frequency solution of Helmholtz equation. Moreover, increasing in two times of diameter of considered specimen on networks with distributed vortices will lead to fourfold increasing the vortex number forcing also the computational problems.

On other hand, in the case of HTSC, computational schemes developed for mesoscopic GL models cannot be directly applied at designing corresponding devices because of existence of great number of vortices. The vortex network in superconductive specimen, for example of millimeter size will consist of great number of vortices due to typical distance of ~ 100 Å between single vortices. At the same time, computational and analytical results used for these media, as rule are based on simple homogenized or macroscopic models, for instance the mean-field models describing the vortex state in terms of the vortex density. Since, the superconductivity is phenomenon, in which quantum–mechanical effects demonstrate macroscopic behavior, then it is obvious that more effective computational schemes for the vortex states could be developed based on multi-scale approach combining, for example the GL model or laws of vortex dynamics with the models of mean field.

In relation to experimental studies, it is known that in the layered cuprate HTSC, the vortex lattice melts in wide range of fields and temperatures. As it has been above noted, at phase diagram of the magnetic states of HTSC are differed

regions of Meissner phase, vortex crystal and vortex liquid. The properties of the magnetic vortex liquid in HTSC remain be studied insufficiently. In particular, the theoretical estimates of melting temperature of the vortex lattice, and also value of energetic barrier preventing to destruction of vortices at their crossing are changed into very wide bounds. The magnetic force microscope could be used for manipulation with single magnetic vortices. In particular, this allows one to "bind" two vortices in some similarity of double DNA spiral. Moreover, by using this microscope, it may be attempted to tear a vortex from pinning center. In a whole, it could be obtained in future by using this method new information on the vortex glass phase, which realized at low temperatures.

2.2.9 Energy Gap Properties of Superconductors

In conventional superconductors the temperature of superconductive transition T_c is directly defined by value of the superconductive gap, Δ, which presents itself an binding energy of two coupled electrons (Cooper pair or pairon) in superconductive state. However, this situation is quite no situation of HTSC, where is absent direct dependence between T_c and Δ. For example, variation of charge carrier concentration can lead to decreasing T_c, but increasing Δ. The value of Δ can be no zero at the $T > T_c$, at the same time in normal state of conventional superconductors always $\Delta = 0$.

The metals become superconductive, when their free electrons divide into the Cooper pairs, at the same time wave functions of all pairs have the same phase. The phase coherence is responsible, in particular for transformation of electric resistance in zero at the cooling lower than the superconductive transition temperature, T_c, and existence in superconductor of the coupled pairs leads to arising gap in spectrum of quasiparticle excitations, which is registered by different spectroscopic methods.

In conventional LTSC the phase coherence of pairs is stated practically simultaneously with their formation, therefore the electric resistance disappears at the $T = T_c$ simultaneously with arising the gap in spectrum. At the same time in HTSC, the gap is conserved also in absence of phase coherence that is in non-superconductive samples. Origin of this gap, called by pseudogap, up to date is subject of discussions. According to one of viewpoints, the pseudogap is caused by presence of coupled, but non-coherent pairs (macroscopic phase coherence is fractured by thermal fluctuations), that is in fact to be portent of superconductivity. Advocates of alternative interpretation assume that the pseudogap forms due to proximity of HTSC to some non-superconductive (possibly, magnetic) state which competes with superconductive one and is to be a sign of existence another type of ordering (for example, spin or charge one). According to two scenarios, in HTSC simultaneously could exist either only one gap (superconducting or pseudogap), or the both together.

At the temperature which is upper some temperature (the temperature of arising of the pseudogap) $T^* > T_c$, the "square-like" Fermi surface (the Fermi contour in *ab*-plane) is observed. Decreasing temperature lower than T^* leads to arising the pseudogap in the electron state density in the Fermi level: in some parts of the Fermi surface, the energy gap presences, at the same time it absences in other sites having shape of segments (so-called, "Fermi arcs") divided one of other. In this case, the electron number in the Fermi surface decreases sharply. At the following cooling the sample down to T_c, the transition in superconducting state occurs, that is in the Fermi surface already arises the superconducting gap. The attempts to experimentally solve this dilemma are complicated by strong anisotropy of the superconductive gap which is zero at "nodes" and maximal at "antinodes". Since, majority spectrographic methods give information either on maximal value of the gap, or its mean value, then distinguishing the great non-superconductive gap in antinode region and small superconductive gap in the rest of part of the Fermi surface is very difficult problem.

Nevertheless, the experiments witness on existence of two different types of the energetic gap in HTSC, namely: charge (it is displayed in spectrum of charge excitations, for instance when is studied single-particle tunneling and relaxation of quasiparticles with time resolution) and spin (it is displayed in spectrum of nuclear magnetic resonance, scattering spin-polarized neutrons and other methods which are to be sensitive to electron spin flip). The pseudogap state is characterized by existence of electron ordering in actual (coordinate) space. This ordering can arise because of pinning the fluctuating incommensurable wave of spin density. Thus, complex phase diagram of the cuprate HTSC (see Sect. 2.2.2) is a sequence of competition between various types of ordering. The energetic gaps are to be dependent both as on doping level of HTSC, as CuO_2 layer number per elementary cell.

Two-dimensional Hubbard model allows one to study main phenomena proper for the superconductive cuprates. At half-filling energetic structure, it defines antiferromagnet Mott–Hubbard state. At introducing doping, the pseudogap arises, and *d*-wave pairing and state with charge stripes (stripe phase, see Sect. 2.2.1) display at low temperature. Various numerical methods have been used to investigate the Hubbard model and *t*–*J* model. The approach, connected with the Lanczos diagonalization of small clusters has been developed in [112, 325, 770, 1005, 1373, 1374], the density matrix by using the renormalization-group method (RGM) for *n*-leg "ladders"[7] has been studied in [326, 617, 1796], quantum

[7] In particular, note that Sr–Ca–Cu–O compounds with so-called "spin ladders" present themselves an analogs of HTSC, because of contain layers of almost one-dimensional "ladders" (that is number of "legs") since they contain layers of almost one-dimensional "ladders" from copper and oxygen atoms. Increasing transverse sizes of this "ladder" (namely, the number of "legs") leads to its gradual development into copper-oxygen plane, which as it is assumed answer for high-temperature superconductivity. It has been theoretically shown that shot-acting spin correlations lead to formation coupled pairs of holes in the "ladders". Superconductivity has been discovered in $(Sr, Ca)_{14}Cu_{24}O_{41}$, while at high pressure.

modeling by using Monte-Carlo method in two-dimensional lattices has been carried out in [49, 205, 1599]. In principle, these methods could be extrapolated to three-dimensional treatment or in the RGM case—to the infinite length of the "ladders". Other important numerical approaches are the extrapolation with zero dispersion based on the Monte-Carlo method [49, 1599], the variation cluster approximations [327, 1073, 1396], the renormalization-group flow techniques [702, 1473], and also high temperature series expansions [914, 1412].

Cluster generalizations of the mean-field dynamical theory [327, 1073, 1396] ensured new information on low-temperature properties of HTSC. Significant advantage of these numerical methods (for instance, in relation to the Hubbard model) consists in that what they are capable to study antiferromagnetism, charge stripes, pseudogap behavior and $d_{x^2-y^2}$-pairing. Moreover, the computational methods have shown as could be balanced these models between almost degenerate phases.

A doping breaking half-filling can displace the balance from antiferromagnetism to the charge state, at which the region bounds with half-filling divide the antiferromagnet regions with phase sheared on π. The stated balance also reveals in different results obtained by using various computational approaches for the same model. For example, RGM for density matrix for t–J "ladder" structures [1796], has stated existence of charge stripes in ground state. However, variation approach and calculations of Green function based on Monte-Carlo method for doped t–J lattice [1599], found ground states characterized by the $d_{x^2-y^2}$-superconductive order at presence of only weak signs of existence of the charge stripes.

The pointed computational methods state modern level of investigations. They can lead to different results, that is direct sequence of various boundary conditions or/and different other aspects of used computational lattices. Open boundary conditions in the RGM-computations of the "ladder" structures can favor to formation of stripe phase. On the contrary, finite sizes of cluster lattices and boundary conditions can prevent from its formation. It is also possible, that these differences reflect imperfection of different numerical methods. Nevertheless, these results, collected together, show that the stripe and $d_{x^2-y^2}$-superconductive phases are to be almost degenerate low-energetic states of doped system.

The quantum modeling by using the Monte-Carlo method [1401] also as different cluster calculations demonstrate that the Hubbard model for underdoped case shows pseudogap states. Tremendous likeness of this behavior with a set of phenomena observed in cuprates provides correct witness that what the Hubbard model and t–J model cover actually significant part of physical essence of given problem. The computational methods have been used to study interaction structure which is responsible for pairing in the Hubbard model. The dependence of superconductive gap on impulse (momentum) and oscillation frequency has been numerically studied in [1495]. The obtained results showed that the pairing interaction in the doped Hubbard model is repulsive into elementary cells, attractive between nearest cells and slowed in time at rearrangement of spin-fluctuation spectrum. It is important to note, that this spectrum includes a

continuum of particles and holes. By this, it is necessary to answer on question, is this interaction actually mechanism responsible for pairing in HTSC, and how learn this from experiment?

Since this issue touches dependence of pairing interaction on impulse then investigations of superconductive gap, fulfilled by using the angle-resolved photoemission spectroscopy (ARPES) [328], together with the transport study [275], and also the phase structure study [1714] ensure strict witness of nodal *d*-wave character of this gap. At the same time, as it has been stated in [876, 1586], existing couples in YBCO lead to admixture of *s*-wave, and studied impulse regions in majority dispose along the Fermi surface. Therefore, based on the observed $\boldsymbol{k}$-dependence of superconductive gap (where $\boldsymbol{k}$ is the wave vector), it may be presented that actually pairing interaction is repulsive into cell and attractive for singlets formed between nearest cells.

Other characteristic of the interaction is its frequency dependence. In relation to it, there is lesser information, however, similar that the frequency dependence of superconductive gap and renormalization parameter can give important contribution in understanding the pairing mechanism for HTSC. It is known, that the frequency dependence of superconductive gap for conventional LTSC has provided identification of phonon exchange pairing mechanism, while some time existed doubts on this connection. In the case of HTSC, it was initially to be assumed that the *d*-wave impulse dependence of superconductive gap should ensure enough exact proof. However, this did not occur. For instance, it is known that exchange by B_{1g}-phonons favors to *d*-wave pairing while its total contribution in superconductive transition temperature T_c is small in accordance with standard theory.

On the other hand, two-level Cu–O-model assuming that fluctuations in circulating currents ensure the mechanism of *d*-wave coupling has been proposed in [1745]. Even, into framework of the Hubbard model, there are different viewpoints on the process dynamics. In the model [44] (see Sect. 2.2.2 in details), it is suggested that the dynamics take place in energetic scale associated with the Mott–Hubbard gap. However, the numerical results [1495] support a picture, in which dominating contribution is caused by excitations of "article-hole" type inside of relatively narrow energetic strip. While the spectrum of these excitations spreads down to zero energy, the main contribution is associated with wide spin-fluctuation continuum [291]. Thus, obviously again the dynamics will important in identification of the superconductivity mechanism.

In addition to traditional electron tunneling and infra-red conductivity, the ARPES measurements ensure important witnesses for frequency dependence of the renormalization parameter and superconductive gap. Therefore, it is important to extend numerical investigations of the Hubbard model in order to compare obtained results with corresponding test data. Finally, in addition to frequency and impulse dependence of pairing interaction, arises issue on its strength. Actual Cu–O structure has additional ways of exchange interaction, and as it has been shown [335] the Hubbard and *t*–*J* models taking into account interactions in cells can lead to stronger pairing correlations.

Nevertheless, the issue on strength of pairing interaction remains to be open. As it has been noted, different numerical methods applied on various grids can witness in one case on *d*-wave pairing, and in other case on existence of charge stripes. Thus, small changes of local parameters could change a correlation nature, and then issue arises on treatment of role of heterogeneities in cuprates. That theory of dynamical heterogeneity, introduced by pairing, has been developed in [882]. In this approach, the pairing caused by repulsive interactions arises as mesoscopic effect, and HTSC phenomena are considered as arising owing to existence of the mesoscopic structures.

The measurements of admixtures in BSCCO by using scanning tunneling microscopy ensured important new information on local modulation of pairing and its strength [1290]. So, development of different numerical methods together with experimentally-theoretical approaches in future will continue to create new knowledge on electronic properties of wide class of the strongly correlated materials.

2.3 High-Temperature Superconductive Oxypnictides

In February 2008, Hosono et al. [806] synthesized a new superconductor $LaO_{1-x}F_xFeAs$ with the temperature of superconductive transition $T_c = 26$ K, so has been discovered a new superconductive family—superconductive oxypnictides.[8] The critical temperature very rapidly rose up to 43 K in $SmO_{1-x}F_xFeAs$, then to 52 K in $PrO_{1-x}F_xFeAs$, and to 55 K in $SmO_{1-x}F_xFeAs$, synthesized under high pressure. The maximal critical temperature $T_c \sim 56$ K has been stated in *M*FFeAs (M = Ca, Sr, Ba, Eu) with superconductivity arising upon modification with Ln^{3+} ions [269, 1809]. That high critical temperature near the liquid nitrogen temperature (77 K) allows us to relate the superconductive oxypnictides to the high-temperature superconductors. Similar to the cuprate HTSC, the fourfold compound LaOFeAs has layered crystalline structure with periods of tetragonal elementary cell $a = 0.40355$ nm and $c = 0.87393$ nm.

As in the cuprate HTSC, where superconductivity occurs in CuO_2 planes, the conductive layers (FeAs) of superconductive oxypnictides are to be spatially divided with the charge reservoir layers (LaO). If in the first discovered superconductive oxypnictides the superconductivity arose at doping of original non-superconductive compound LaOFeAs by electrons (by the way of O substitution on $O_{1-x}F_x$), then later it was became to be clear, that hole doping (at the La substitution on $La_{1-x}Sr_x$) also leads to superconductivity. Thus, in this relation the high-temperature oxide superconductors without copper lead themselves similarly to their cuprate analogues.

[8] Pnictides are compounds containing elements of Mendeleev periodical table of chemical elements such as, nitrogen, phosphorus, arsenic, etc.

However, their "parent" states are to be different. If non-doped cuprates are to be dielectrics (antiferromagnetic or Mott ones), then underdoped oxypnictides present themselves either non-magnetic metals or antiferromagnetic semimetals. According to that, there are two principle differences of oxypnictides from cuprates, namely: (i) magnetism of parent non-superconductive phase in the first case is caused by de-localized electrons, but in the second case—by local magnetic moments, and (ii) the superconductivity of HTSC cuprates arises only due to "chemical doping" (non-isovalent substitution of some elements by others or change of oxygen concentration), at the same time the superconductivity of HTSC oxypnictides arises additionally under influence of high pressure. Thus, the doping and strong compression by the same way changes definite properties of the superconductive oxypnictides which are significant for their superconductivity.

The effects of doping (Ba $\rightarrow$ $Ba_{1-x}K_x$) and pressure ($T_c = 31$ K at the $p = 5.5$ GPa) on structure of $BaFe_2As_2$ have been studied by using the neutron diffraction [871]. In both cases, occurred shortening length of couple Fe–Fe and angle As–Fe–As, and also suppression of transition from tetragonal to orthorhombic phase. These changes of crystalline structure, in its turn led to change of electronic structure. The performed calculations showed that at the doping and pressure increasing, the shape of energetic zones changes in vicinity of the Fermi level, nesting the Fermi surface weakens and the spin-density wave (SDW) destabilizes. Therefore, it has been made a conclusion that the main factor, defining superconductivity of the oxypnictides, was connected (in difference of cuprates) no concentration of moved carriers, but a kind of electronic zone structure.

Information on superconductivity of undoped compound $SrFe_2As_2$ has been presented in [690]. First, the thin films of $SrFe_2As_2$, received by laser evaporation, as it could be expected to be non-superconductive. However, at the repeated measurements performed after some hours, they demonstrated superconductive transition at the $T_c = 26$ K. All this time the films be kept at air and the cause of the cardinal change of the electric properties was caused by water steams penetrated into the films from environment atmosphere. As it was elucidated, the water penetration into $SrFe_2As_2$ caused a convergence of atomic layers and arising superconductivity. On the one hand, explanation of this phenomenon can be a key to the superconductivity mechanism of without-copper HTSC, and on the other hand, can prompt a way to increase their critical temperature.

Investigations of structure and magnetic characteristics of LaOFeAs by using neutron diffraction method [346] showed that at the decreasing temperature, first at the $T = 155$ K occurred structural transition from tetragonal to monoclinic phase, and then at the $T = 137$ K, it was formed far antiferromagnetic order with SDW. The substitution of O on $O_{0.92}F_{0.08}$ suppressed both these transitions and led to superconductivity with $T_c = 26$ K. Thus, as in superconductive oxypnictides, as in cuprate HTSC, superconductive state adjacent with antiferromegnetic, that gives some arguments to speak on non-phonon mechanism of pairing carriers in the both superconductive families.

The studies of structure and magnetic phase diagram of $CeFeAsO_{1-x}F_x$ into coordinates "temperature—concentration of charge carriers" [1875] by using

neutron spectroscopy method showed that similarly to HTSC, the temperature of structural transition in oxypnictides becomes zero at the carrier concentration corresponding to maximum of T_c. At the same time, there is important difference of the phase diagrams of cuprates and oxypnictides, namely: in latter value of T_c, attaining at doping itself maximum, then very slowly decreases but does not turn into zero, that what overdoped non-superconductive state in their phase diagram is absent.

The measurements of temperature dependence of high critical magnetic field H_{c2} in $LaO_{0.89}F_{0.11}FeAs$ [730] showed that the value of $H_{c2}(0) \sim 65$ T was significantly greater than it may be expected for single zone superconductor on the base of value of the derivative $dH_{c2}/dT \sim 2$ T/K near T_c. Based on this result, it has been made a conclusion on two-zone superconductivity of oxypnictides as in MgB_2. However, studies of value of the superconductive gap D in $SmO_{0.85}F_{0.15}$-FeAs by using Andreev spectroscopy [267] led to the contrast conclusion on single zone superconductivity. The calculated value of $2D/(k_BT_c) = 3.68$ (where k_B is the Boltzmann constant) was very closely to corresponding value (3.53), obtained on the base of the BCS-theory. More that, the temperature dependence, $D(T)$, into all range $0 < T < T_c$ very good agreed with the BCS-theory. In this case, it may speak on involvement to superconductivity some bosonic excitations.

It may be affirmed, that the parameter of superconducting order in oxypnictides has not zeros on the Fermi surface in difference of the cuprate HTSC. Moreover, any pseudogap features also even have not discovered. In spite of their layered crystalline structure, oxypnictides demonstrate practically isotropic superconductivity. On that behavior results witness which have been received at the study of monocrystals (Ba, K)Fe_2As_2 into magnetic field of approximately 60 T [1852]. It has been elucidated, that in a whole temperature range lower than T_c, the value of H_{c2} is independent almost of direction of magnetic field that sharply contrasts with all known layered superconductors. The probable cause of the H_{c2} isotropy may be isotropy of the Fermi surface, but test data on its topology remain to be contradictory.

The Fermi surface of (Ba, K)Fe_2As_2 has been studied by using ARPES [1860], where shown its anisotropy even into *ab*-plane, in which it had a shape of "propeller" that differed of zone calculations. These authors assumed that their results could be explained by presence in superconducting oxypnictides some electronic order co-existing with superconductivity and keeping up to 300 K. It is not usual charge-density wave (CDW), but something more complex reminding hypothetical "hidden order" in cuprates. Underdoped oxypnictides being either non-magnetic metals or antiferromagnetic semimetals demonstrate magnetic properties which are expressed far weakly than at cuprates. They are very sensitive to smallest changes of crystalline structure and chemical composition that strongly impedes an interpretation of test data.

In [1108], it has been expressed proposition supported by calculations and tests on that, what magnetism of the HTSC without copper is caused by new type of magnetic excitations that is "magnetic antiphasons", which are connected with antiphase boundaries between regions with local SDW-order. Fast fluctuations of

these excitations could lead to that, what a result of any experiment depends on corresponding time scale. The conception of antiphasons allows one to give natural explanation the temperature difference of structural and magnetic transitions in oxypnictides.

In [1034], it has been studied an influence of isotopic substitution of $^{18}O/^{16}O$ and $^{56}Fe/^{54}Fe$ on T_c of two typical representatives of the HTSC without copper, namely $Ba_{1-x}K_xFe_2As_2$ with $x = 0.4$ and $SmFeAsO_{1-x}F_x$ with $x = 0.15$. For oxygen, the factor $a = -d(\ln T_c)/d(\ln M)$ (where M is the isotope mass), characterizing isotopic shear of T_c, turn out to be very small (about 0.05), at the same time for iron $a \approx 0.35$, that to be closely to "phonon standard" ($a = 0.5$). In these tests, it has been also studied as isotopic substitution influences on the transition temperature T_{SDW} of original compounds with $x = 0$ into state with spin-density wave. The corresponding value of $a_{SDW} = -d(\ln T_{SDW})/d(\ln M) \approx 0.05$ and ≈ 0.37 has been calculated for oxygen and iron, respectively.

In absence today, common theory of influence of the isotopic substitution on magnetic phase transitions, these results could be interpreted differently. From the one hand, the great value of a witnesses on that, what electron–phonon interaction plays definite role in superconductivity of oxypnictides, and from the other hand, it is obvious presence of strong phonon-magnon interaction. Therefore, it is quite possible, that the isotopic change of T_c is connected with change no phonon, but magnon spectrum of superconductive oxypnictides. Proper details of non-phonon coupling mechanism for account of carrier interaction with magnetic excitations are defined by microscopic nature of antiferromagnetic state. If magnetism in cuprates is caused by ordering local magnetic moments and well described by Heisenberg model, then the data on antiferromagnetic order in pnictides remain to be contradictory: some experiments witness on its local character, at the same time the others speak on definite role of collectivized electrons (as in metallic chrome).

An elastic scattering of neutrons on monocrystals of $CaFe_2As_2$ has been studied and it showed that from the one hand, dispersion of spin waves in a whole Brillouin zone of this "progenitor" of the superconductive oxypnictides is described by the Heisenberg model (in which are taken into account exchange interactions between nearest and following for the nearest neighbors) [1874]. From the other hand, very strong difference of interaction energies along a- and b-directions of Fe–As–Fe layers could not be explained, if account of all orbitals of Fe-atoms be localized. So, magnetism of pnictides is not to be purely local or purely collectivized, but presents itself a complex mix of the both types.

As it has been noted, the common structural elements for oxypnictides are to be conductive layers of FeAs. The layers from other atoms stabilize crystalline lattice and are to be sources of current carriers. Namely these layers (various for different pnictides) are responsible for a set of specific effects which have not relation to superconductivity, for example for phase delamination. They significantly complicate a picture and are difficult to an interpretation of test data. The idea to get rid of these layers led to study of iron chalcogenides FeX (X = S, Se, Te), related to pnictides, in especially iron selenides FeSe, a possibility of superconductivity in which has been predicted theoretically [1620]. It has been stated that FeSe,

no containing "excess" layers, has very low T_c (about 8 K), and therefore a doubt arose on that, what it could be treated as a ground compound for study of superconductivity of oxypnictides [712].

However, in [1123], it has been shown, that FeSe becomes high-temperature superconductor at enough high pressure, p. In this compound, the value of T_c increases rapidly with growth of p (it is possible because of increasing carrier concentration in FeSe layers) and attains 37 K at the $p = 9$ GPa (it is almost record for binary superconductors). In difference of cuprate HTSC and compounds with heavy fermions, superconductivity of FeSe at the following increasing p disappears does not because of exceeding optimal carrier concentration, but because of structural transition into hexagonal phase. If this transition will be avoided, then maximal T_c will be significantly increased. It has been also stated absence in FeSe of static magnetism at all values of p (in majority of undoped pnictides takes place a static magnetic order, which changes by superconductivity at doping or increasing p). Therefore, the growth of T_c under pressure is not connected with suppression of competing magnetic order. However, it does not sign, that magnetism has nothing to do superconductivity of FeSe. Data of nuclear magnetic resonance, received in [743] witness on presence of spin fluctuations in superconductive state of FeSe, which in principle could be responsible for the Cooper pairing.

2.4 Future Studies of High-Temperature Superconductivity Mechanism

From "electronic view", the main problem of construction of unified model consists in that what electrons in HTSC cannot considered separately: each of them interacts with others that is the given system to be "strongly correlated". The general methods, describing these systems until are to be only at the stage of development. Nevertheless, several theorists are believed that the electron pairing in HTSC occurs (as in usual BCS-superconductors) for account of their interaction with oscillations of crystalline lattice (phonons). Others insist on "magnetic mechanism" of pairing. Thirds assumes that the key could be found in charge heterogeneities (stripes, etc.). It should not be excluded some combination of all above factors.

One of the HTSC "fathers", Nobel Laureate, 1987—Müller to be so far convinced in polaron mechanism of high-temperature. Nobel Laureate, 2003 in the region of superfluidity—Leggett assumes that nearest goal of experimental studies should be statement as the causes of the property universality of various superconductive families (for example, similar dependence of the critical temperature T_c on number of the CuO_2 layers per elementary cell), as the causes of their non-universality (for example, sharp T_c-difference of single-layered HTSC based on Hg and Tl), and also clarification of role of the high-energetic excitations in HTSC

superconductivity. Now, he develops a scenario for cuprate superconductivity in which a major factor is the reduction, due to increased screening by the Cooper pairs, of the long-wavelength, mid-infrared-frequency part of the Coulomb interaction. In addition, independently of this scenario, he attempts to explain the *c*-axis transport properties of the cuprates and look at some problems associated with the "pseudogap" regime and with the peculiar features resulting from the existence of gap nodes. Nobel Laureate, 1977—Anderson is faithful his RVB theory and assumes that it (may be with some modifications) can explain an essence of HTSC phenomenon. Now he focuses on achieving understanding of the crucial experimental anomalies in HTSC behavior. In his opinion, the key to the problem is a new method of dealing with the constrained Hilbert space which follows from the necessity of the Gutzwiller projection. Rice and Lee have the same opinion, and the last hopes that it will be success (at least by using numerical calculations) to prove existence of superconductivity in Hubbard model with repulsion. Pines is also convinced in non-phonon mechanism of HTSC superconductivity. From his view, we are near coordinated microscopic theory of superconductivity of overdoped HTSC which should be based on accurate description of electron interaction with antiferromagnetic fluctuations. However, in this case, it is necessary to understand why at the doping other antiferromagnetic dielectrics (for example, $LaTiO_3$, V_2O_3, NiS_2, Sr_2VO_4), a superconductivity does not arise even at the very low temperatures (in this fact pays attention Imada). Zaanen considers that HTSCs differ not their complexity, but on the contrary—simplicity which is displayed, for instance in strictly linear temperature dependence of electric resistance of the optimally doped samples upon to the melting point. This cannot be a simple accidence. Therefore, it is necessary to shun any dogmas, for instance as dogma of Anderson–Hubbard on electronic mechanism of HTSC superconductivity. Obviously, phonons play an important role while highly unusual with positions of microscopic theory. It is required to search basic principle laying in the basis of the phenomena. The key could be given by experiment. Chakravarty sees this key in a "dome"-like dependence of T_c on number of the CuO_2 layers per elementary cell, but Senthil is based on proximity of superconductive, dielectric (Mott's) and pseudogap states. Randeira attaches a great importance to search in HTSC new elementary excitations with unusual quantum numbers and detail analysis competition between different ordered states.

Thus, in relation to HTSC theory can be selected two polar positions, namely: (i) numerous unusual HTSC properties are caused by various no connected between them effects, that what can speak, for example on the theory of transport properties and theory of the pairing mechanism as on two different theories, (ii) natural explanation of all features of HTSC could be given from united view into framework of new theory of condensed matter with strong correlations. Schmalian supports the second view and assumes that systematic phenomenology of several HTSC families speaks in its favor. However, even it is not completely to be clear, as suggests Vojta, do these character features as pseudogap, stripes and heterogeneities observed by scanning tunnel microscopy to be necessary ingredients or on the contrary obstacle for high-temperature superconductivity. Varma thinks that

experiment supports predicted by him the breaking symmetry relatively a time reversal in the pseudogap phase for account of spontaneous arising closed contours with current in CuO_2 layers. Therefore, the pairing charge carriers and anomalous properties of HTSC above T_c are caused by strong fluctuations in vicinity of quantum critical point, where the pseudogap "closes". Davis assumes that for solution the HTSC problem completely, it is necessary in a whole to understand the HTSC phase diagram but not only to study the superconductivity mechanism.

The above wide scattering of opinions of the leading scientists in the region of HTSC demonstrates a reality of existing discords which must be removed for statement of complete mechanism of high-temperature superconductivity. Today, the high-temperature superconductivity could be considered not only as one of non-discovered mystery of modern physics, but as a some polygon for selection ideas and methods to describe strongly correlated electrons and a barrier separating researches from principally novel physical concepts.

2.5 Weak Links and Josephson Junctions

In 1962, Josephson published a theoretical paper [796] predicting the existence of two remarkable effects. One was supposed to find them in superconducting tunnel junctions. The basic idea of the *first effect* was that a tunnel transition should be able to sustain a superconducting (i.e., zero-voltage) current. The critical value of this current was predicted to depend on the external magnetic field in a very unusual way. If the current exceeds the critical value, which is a characteristic of a particular junction, the junction begins to generate high-frequency electromagnetic waves. This phenomenon was called *second Josephson effect*.

Soon after their discovery, both effects obtained experimental confirmation [1547, 1831]. Moreover, it soon became clear that the Josephson effects exist not only in tunnel junctions, but also in other kinds of the so-called weak links, in particular, short sections of superconducting circuits, where the critical current is substantially suppressed [1021, 1022, 1597]. So, initiating weak superconductivity is based on the quantum nature of the superconducting state that assumes the existence of condensate of the Cooper pairs. This means that all electron pairs in the superconducting state occupy the same quantum level and are described by a single wave function, common to all of them. Their behavior is mutually conditioned and they are coherent.

Consider two bulk superconductors having the same temperature and completely isolated from each other. The behavior of the superconducting electrons in each of them is subjected to own wave function, when they are in the superconducting state. Then, because the temperatures and the materials of the superconductors are identical, the amplitudes of the wave functions must also be the same. However, the phases, in this case, are different. This situation remains as long as the superconductors are isolated from each other. Let us establish a weak contact between them, that is, the contact which is weak enough so as not to change

radically the electron states of the two superconductors, but sufficient to initiate a perturbation. In this case, a new wave function is formed that is general for the joint superconductor, which can be considered as a result of interference between the wave functions of both its pieces. Therefore, phase coherence is a direct result of establishing the weak link.

In first stage of R&D of the high-temperature superconductive Josephson junctions (HTSC JJs) it has been assumed that main difficulties of their processing are connected with technologies. Due to the very small coherence length (several angstroms) in HTSC-materials, in order to receive qualitative and reproduced on parameters of the Josephson junctions, were required to solve three technological problems: (i) to grow epitaxial HTSC-films and multilayered structures (ii) to form a necessary structure of the film, and (iii) to carry out a control of boundaries in atomic scale. With these aims the unique processing methods of strontium titanate, sapphire, and neodymium gallate have been developed. Namely on these substrates have been processed the record on their noise characteristics HTSC JJs. SQUIDs manufactured on these substrates have record parameters at 77 K: sensitivity on magnetic flux $2.5 \cdot 10^{-5}$ $\Phi_0/\mathrm{Hz}^{1/2}$ (on frequencies upper of 30 Hz), cutoff frequency noise $1/f \sim 10$ Hz, depth of output signal modulation up to 120 μV.

However, the required homogeneity of parameters for relatively complex devices consisting of several tens of HTSC JJs has not been attained. During time, it became to be clear, that the problem of homogeneity and reproduction of parameters has ground physical nature being a sequence of anisotropic pairing which is intrinsic for HTSC (different of traditional type for LTSC) *d*-coupling. It is known that the *d*-coupling is very sensitive to electron scattering on admixtures and suppresses at the comparatively small their concentrations. However, interior of HTSC, defects localize in interplane positions, due to transport properties in superconducting CuO_2-planes correspond with well accuracy to condition of pure limit.

The situation changes cardinally in vicinity of intergrain boundaries or artificially created interfaces of JJs. As a result of electron scattering on boundaries and defects, localized in their vicinities, the partial or total suppression of the pairing in *d*-channel occurs, accompanied by arising *s*-type superconductivity. This takes place owing to the electron, which incidents on the boundary from the region with positive potential of superconductive coupling, could in a result of the scattering chances to find oneself in the region of space with negative potential. It is qualitatively clearly, that this replacement of sign suggests presence of region, in which density of Cooper pairs crosses zero, at least on these quasiparticle paths. The fraction of these paths, and hence a degree of suppression of the superconductive properties by the boundary depends on the angle between normal to the boundary and crystallographic axes situated into CuO-planes. If these two directions coincide, then the suppression is absent. However, if the angle between them equals to 45°, then the value of the coupling potential on the boundary is strictly equal to zero. This local suppression of superconductive properties is accompanied by arising anomalously great normal conductivity in the region of small stresses, generation of Andreev coupled states at finite energies that is

influences not only on local value of critical current, but on parameters responsible for transport of normal electrons.

In developed, today types of HTSC JJs (the junctions on bi-crystalline substrates, edge junctions, junctions received in a result of modification of the HTSC material properties, caused by any influence), a control for local value of the angle between normal to boundary and crystallographic axes is to be practically impossible. As a result, there is heterogeneity of parameters responsible for transport both superconductive and normal components of current. Therefore, the problem solution in this case lies in creation of technology which is able to manipulate atomic-smooth boundaries.

2.5.1 Classification of Josephson Junctions

The weak links (Josephson junctions, JJs) can be classified in the following way:

(1) *Devices without concentration of current such as tunnel junctions of the "superconductor–insulator–superconductor" type* (S–I–S) (Fig. 2.12a). The thickness of an insulating layer, as a rule, is about 1–2 nm, and the critical current density is in the order of 10^4 A/cm^2, that is, much less than the critical current density of the bulk superconductor, in particular, exceeding 10^5 A/cm^2 at 77 K and 0 T in Y(*RE*)BCO melt-processed samples.[9]

(2) *Layered structure of the "superconductor–normal metal–superconductor" type* (S–N–S). It involves the normal layer with thickness of ~ 1 μm (Fig. 2.12b). The wave functions of the superconducting electrons penetrate the normal metal due to the proximity effect. In the region of their overlapping, the wave functions interfere, establishing phase coherence between bulk superconductors. If the amplitude of the superconducting wave function in the weak link is small, then the critical current is also small.

(3) *Layered structures where a normal layer between two superconductors is replaced by a doped semiconductor or another superconductor with a small critical current density.* For example, if a narrow superconducting film is covered by thin film of a normal metal (Fig. 2.12c), then the amplitude of the superconducting electron wave function in the film is reduced, where the film contacts with normal metal, due to proximity effect. This causes local decrease of the critical current density, that is, weak link formation.

(4) *Devices with concentration of current.* The critical current density in the weak link is the same as in the bulk, but the absolute value of the critical current is much lesser. A superconducting film with a short narrow constriction (Dayem bridge) falls into this category, provided the size of the constriction is of the order of the coherence length, ξ (see Fig. 2.12d). Another example is a bridge

[9] High-quality tunnel Josephson junctions, made of niobium with a barrier layer of aluminum oxide, attain the critical current density of $\sim 10^4$–10^5 A/cm^2.

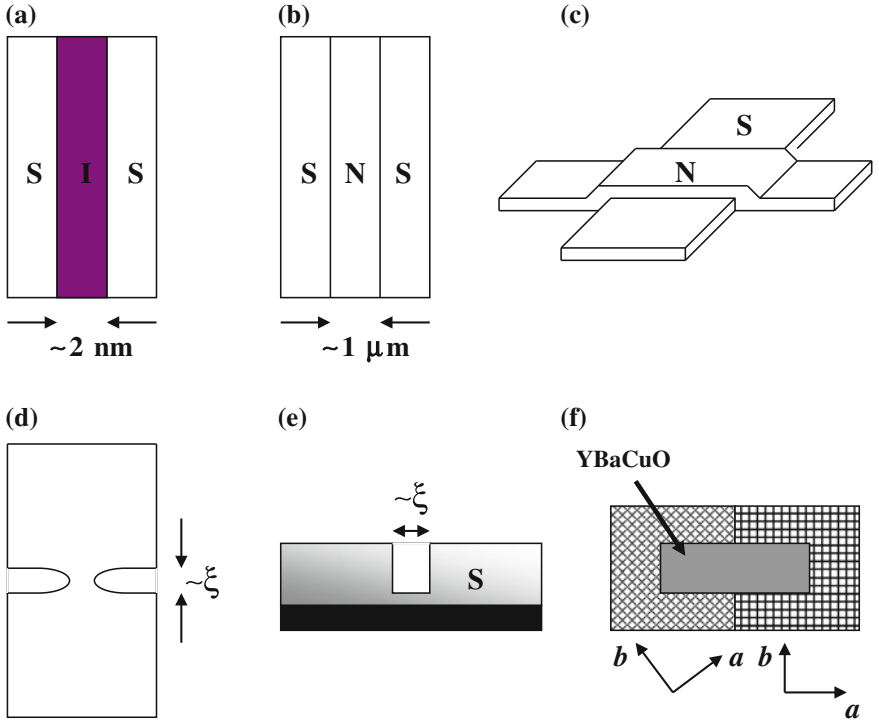

Fig. 2.12 Different types of weak links: (**a**) tunnel junction (S–I–S); (**b**) sandwich structure (S–N–S); (**c**) normal film (N) causes local suppression of the order parameter of superconducting film (S); (**d**) Dayem bridge; (**e**) bridge of variable thickness (longitudinal cross-section); (**f**) grain-boundary junction

of variable thickness, such that the thickness of the basic film is hundreds of nanometers, at the same time, the thickness of the bridge itself equals to only several tens of nanometers (Fig. 2.12e).

(5) *Grain boundary (or bicrystal) transition.* It is a typical one for high-temperature superconductors (Fig. 2.12f). Due to the extremely short coherence length in HTSC ($\xi \sim 1$ nm), defects in their crystalline structure can act as weak links. The best-controlled defects can be produced between two regions of an epitaxial high- temperature superconductive film with various crystal orientations (grain boundaries). The critical current density of such a weak link can be varied, changing the misorientation angle between two crystallites.

HTSC Josephson junctions can also be classified into the following three classes [583]:

(i) junctions without interfaces, in which the weak coupling is achieved by locally degrading the superconducting properties of a HTSC thin-film microbridges by focused electron or ion beam irradiation;

(ii) junctions with intrinsic barriers or interfaces formed, for example, using the intercrystalline boundaries of different crystallographic orientations;
(iii) junctions with extrinsic interfaces, in fabrication of which artificial barriers from normal metals and insulators are used.

From the standpoint of the damage and material strength problem, the last two classes of the Josephson junctions display most interest. HTSC JJs with extrinsic interfaces are prepared by using the film technology, and they themselves present multi-layered structures (hetero-structures) with rectilinear and inclined interfaces. There are different technological possibilities, which are discussed in detail in the following two chapters, for increasing superconducting properties of these systems. For example, an overdoping by calcium of intergranular boundaries in multi-layered structures and YBCO super-lattices permits to significantly increase J_c at all temperatures up to T_c, but also at magnetic fields up to 3 T [331].

2.5.2 Tunneling Junctions Based on High-Temperature Superconductors

In difference of conventional LTSC, clear difference between tunnel junctions and structures with directed conductivity does not preserve for HTSC JJs. Except several cases (for instance, by using scanning tunneling microscopy), a barrier occupies often intermediate site between tunnel and immediate contact. Below, we present main directions of R&D of the HTSC tunneling junctions.

2.5.2.1 Junctions with Single Crystals

First HTSC JJs could not be processed on high-qualitative films and used one of the concepts: (i) bulk materials as electrodes (ii) are manufactured at break junctions, in which bulk part could be divided into two parts at low temperatures (iii) junctions with point contact, in which one of electrodes to be sharp tip. The latter technology applied widely in the past years for conventional Josephson junctions. Creation of first break junctions and junctions with point contact generally was checked by quality of used single crystals and always characterized by bad reproduction of natural barrier in systems with intrinsic complex properties, for instance HTSC. Subsequent significant achievements became to be possible due to technologies of studying surfaces after precipitation (or deposition) artificial barrier and counter electrode (normal metal or LTSC) which allowed one to overcome critical stage of precipitation of the artificial barrier. These approaches have been successively applied to measurement of energetic gap [611] and investigation of order symmetry in YBCO [1805].

2.5.2.2 Grain-Boundary Junctions

This type of junctions [680] demonstrates advantage to significantly decrease critical current between two grains of different orientation which forms a weak couple and behavior of Josephson type between electrodes. Natural existing barrier allows one to overcome the problems which are intrinsic to artificial barriers. These contacts in spite of pointed below shortcomings could be assumed to be high-qualitative and have been formed in a set of experiments.

The critical current on the grain boundaries decreases exponentially with increasing their disorientation angle. This could be roughly interpreted as increasing thickness of the grain-boundary barrier with increasing the disorientation angle, θ. Majority existing data relate to YBCO-transitions however similar angle dependences of critical current density on the grain boundaries have been published for all other HTSCs including electron-doped materials. The terminology used for description of the grain-boundary junctions differs asymmetric case, at which one grain is aligned crystallographically with boundary (Fig. 2.13a) and symmetric case when crystallographic misorientations of two grains relatively of the grain boundary coincide (Fig. 2.13b). For example, the 45° symmetric boundary relates to the 22.5–22.5° misorientations, at the same time, the asymmetric boundary corresponds to the 0–45° misorientations. The 90° boundaries are to be proper partial case, which, for instance takes place in *a*-axis oriented thin films.

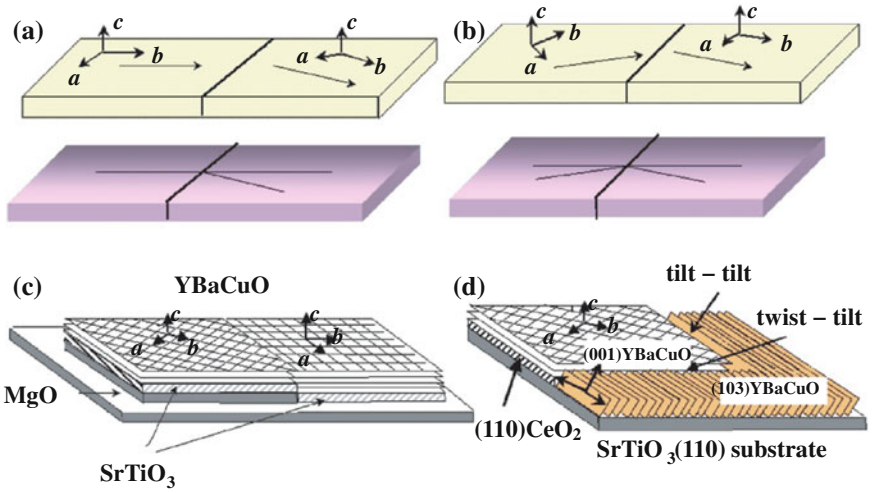

Fig. 2.13 Sketch of bicrystal junction in asymmetric (**a**) and symmetric (**b**) configuration, and of the grain boundary structures in classical biepitaxial (**c**) and CeO_2-based (**d**) out-of-plane biepitaxial junctions. In (**d**) the two limit configurations, tilt and twist, are indicated. In (**d**) the presence of the CeO_2 produces an additional 45° in-plane rotation of the YBCO axes with respect to the in-plane directions of the substrate [875]

Bicrystal technology used for processing the *bicrystal junctions* is based on unification of two substrates with different crystallographic orientations. This technology [1080] directly leads to creation of grain-boundary transitions. Epitaxial HTSC-films reproduce relative orientations of two substrates. Used turn of YBCO axes on relation to corresponding directions into substrate plane is a method of changing relative all-possible orientations of electrodes. Much less, the *c*-axis inclined grain boundaries are used. The bicrystal substrates have been processed on the base of numerous compounds, including $SrTiO_3$, doped $SrTiO_3$, MgO, zirconium, yttria-stabilized zirconia, YSZ), $NdGaO_3$, $LaAlO_3$, Si, etc. [584, 680, 762]. Other technologies (step, step-edge and biepitaxial) can overcome restrictions introduced by bi-, three- or tetracrystalline substrate in sites of the contact disposition. All other technologies apply means of lithography to state interfaces based on the grain boundaries. While they are more optimal for creation of junctions used in basic researches and more effective for designed electric circuits, however the grain boundaries based on these technologies are restricted by specific disorder angles and processing some of these junctions could be sufficiently complex.

Biepitaxial junctions use changes of orientation of HTSC-films introduced due to epitaxial growth on structured model layers. In original technology [257], model MgO layer on sapphire *r*-plane turned into plane on angle 45° to double layer of $SrTiO_3$/YBCO (Fig. 2.13c). Subsequent works used various material combinations in order to introduce alterations in orientation into plane. In the following years it has been modified biepitaxial technology for receiving new configurations [1641], in which one of the electrodes did not turn along *c*-axis. Specific feature of these structures is use (110)-oriented buffer layer of MgO or CeO_2 (Fig. 2.13d), deposited on (110) $SrTiO_3$-substrate. YBCO grew along [001]-direction on seeding layers of MgO and CeO_2.At the same time, it grew along [102]/[013]-direction on $SrTiO_3$-substrates. Presence of CeO_2 created additional 45°-turn of YBCO-axes into plane relatively of the substrate directions in the same plane. Due to this the grain boundaries were a product of two 45°-turns, first of which performed around *c*-axis, and second—around *b*-axis. This configuration led to required 45°-misorientation between two electrodes, which is necessary to increase *d*-wave effects of order parameter. Biepitaxial intergranular boundaries possess lesser probability of transport compared to other types of grain boundaries and to be nearer to the tunnel limit. Apparently, it was a key feature which led to first successive observation of angle dependence of critical current I_c in HTSC-junctions [1043], and first observation of macroscopic quantum tunneling and quantization of energetic levels in HTSC JJs [105, 106].

2.5.2.3 Step-Edge Junctions

The grain boundaries also form during growth of HTSC-film upper step duly formed inside substrate. The resulting structure depends on the step morphology. However, a boundary of one grain, as rule born on the step bottom, but other

grain—on its upper part, and they couple electrically. The step-edge junctions could be disposed at any site of substrate that is found by lithography possibilities (in majority using amorphous carbon mask and ion-ray etching and reactive ion etching). The step height (200–300 nm) is usually greater than film thickness, at the same time both the step edge and substrate material plays decisive role. Better fulfillment is achieved for great angles of the step. The problem of reproduction is a serious restriction for using these junctions in various applications.

2.5.2.4 Electron Beam Junctions

As it has been noted above, the Josephson junctions also processed by using weakening superconductive properties in narrow microbrodges. With this aim, various sources of irradiation (in particular, electronic) are used. In HTSC, the irradiation creates displacement defects acting as scattering centers into Cu–O-planes and being mostly by oxygen defects for energies of order 100 keV. At the higher irradiation energy (>300 keV) could be created defects on copper. Decreasing concentration of charge carriers (due to, for instance removal of oxygen links at the diminished irradiation energies) decreases the doping level that leads to decreasing critical temperature, T_c. The irradiated barrier region during using this technology is no subjected never to air influence or fracture. Co-focused electron-beam irradiation is used also for modification of properties of the grain-boundary JJ. In this case, the situation becomes more complex due to presence of grain boundary acting as drain of defect migration defining kinetics of their accumulation. The irradiation by electrons changes volt-ampere characteristic, and apparently barrier also as the grain-boundary microstructure at the change of oxygen content in vicinity of these interfaces. These changes could be controlled altering electronic doze and partially restored by isothermal annealing of the junction. Other examples of the corrected barriers are connected with irradiation by protons and light which lead to decreasing I_c and increasing R_n similarly to the irradiation by electrons. Usually, the results are interpreted in terms of the barrier height of tunneling in dependence on physical influence.

2.5.2.5 Junctions with Artificial Barriers

While the grain-boundary junctions are only based on thin films, the junctions with artificial barriers have been processed as on the base of thin film as single crystals. It is obvious that the junctions based on single crystals have scientific interest only for basic experiments. For example, first junctions "YBCO single crystal-Pb (Nb) insulator" [611] have been rapidly replaced by second generation, based on thin films [832]. The barriers have been processed by using different methods, and as the barrier materials used noble metals and oxides. Various geometries and electrodes are used corresponding with selection of advantages and different features (greater coherence length, anisotropy, etc.). For instance, the ramp-edge

junctions are manufactured by using well-developed *c*-axis HTSC thin-film technique allowing flow of transport current into *ab*-planes. The optimization of the interface electric resistance advanced a research activity directed to development of oxide barriers. The interface resistance could be caused by discrepancies of carrier density, lattice constants, thermal expansion and dimension. This has been moving force for development of strategies directed to decreasing the lattice discrepancy including agreement of the thermal expansion factors in direction of *c*-axis (PrBaCuO and Pr-doped YBCO), increasing the carrier density and displacement of YBCO into region of increased doping (Ca-doped YBCO), decreasing the carrier concentration at cation substitution of places in crystalline lattice far of CuO_2 planes ($YBa_2(Cu_{1-x}Co_x)_3O_{7-x}$) and substitution of Cu-atoms immediately into CuO_2 planes by using, for instance Zn or Ni [51].

2.5.2.6 Noble Metal Barriers

Gold and silver have been used as barriers for junctions based on single crystals and thin films because of their well compatibility with HTSC. Different counterelectrodes (as low-temperature superconductive as high-temperature superconductive) and configurations have been used together with HTSC as ground electrode. HTSC-junctions of S–N–S type (where S is the superconductor and N is the normal metal) in ramp-edge geometry have been processed by using special layers introduced with aim to possess proper division of superconductive electrodes and state a conductivity of the junction via barrier from gold. Focused ionic radiation has been applied to create narrow grooves, where occurred natural

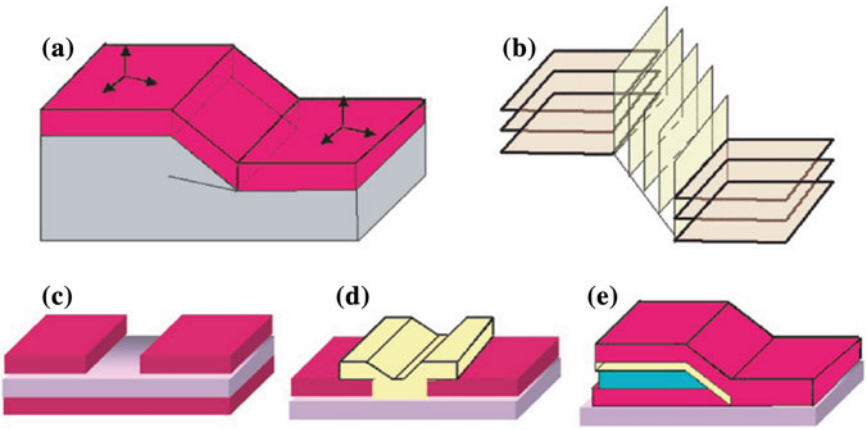

Fig. 2.14 (**a**) and (**b**) step junctions for high α angles (**c**) and (**d**) SNS coplanar junctions; in (**c**) the barrier is predeposited or occurs through a suitable substrate while in (**d**) the normal metal barrier is deposited in a narrow trench; (**e**) SNS ramp-edge junction: in improved versions a degraded layer of YBCO next to the Au is eliminated through suitable surface treatment before in situ deposition of the Au barrier and Nb counterelectrode [1585, 1587]

breaking YBCO films. The junctions with LTSC counter-electrodes are often simpler in processing than corresponding samples based on HTSC thin films however they have restricted range of work temperatures.

The processing technique of ramp-edge junctions [1587] (Fig. 2.14e) allowed one to use photolithography to process high-quality junctions. In this technique the ramp edges prepared on the base of [001]-oriented YBCO-films by using pulsed laser deposition (PLD) by using photolithography and ionic etching in argon. The devices have been etched and cleared, and then thin layers of YBCO and Au deposited by using PLD in situ. The junction processing has been finished by applying of Nb layer. This process eliminated the defective layer of YBCO sequent for Au improving the junction characteristics. This technique has been used for processing junctions with specific verges reproducing unusual magnetic interference pictures displaying in asymmetric 0–45° grain-boundary junctions and with aim to obtain great arrays of π-rings applied in π-SQUIDs.

2.5.2.7 Barriers Based on Perovskites and Layered Materials

Comparative investigations between cubic perovskite barrier materials ($CaRuO_3$, $SrRuO_3$, $La_{0.5}Sr_{0.5}CoO_3$) and layered materials ($Y_{0.7}Ca_{0.3}Ba_2Cu_3O_{7-x}$, $YBa_2Cu_{2.79}Co_{0.21}O_{7-x}$, $La_{1.4}Sr_{0.6}CuO_4$) have been carried out in junctions with ramp-edge geometry [52]. Deficiency/disorder of oxygen has been studied as a source of electric resistance of interface [256]. In the case of cubic perovskite barriers, characterized greater difference of the thermal expansion factors compared with YBCO, the greater values of resistance have been obtained in normal state of the material ($R_nA \sim 10^{-8}\ \Omega{\cdot}cm^2$) than corresponding values for layered materials ($R_nA \sim 10^{-10}\ \Omega\ cm^2$). For YBCO samples, doped by Co (Ca), being overdoped (underdoped) versions of YBCO with greater (lesser) carrier density, lesser critical temperature, T_c, and lesser (greater) anisotropy than YBCO, have been received comparative results. In [51, 354], it has been shown that the proximity effect had place for the both types of barriers. PrBaCuO and oxides based on Pr-doped YBCO ($Y_{0.3}Pr_{0.7}Ba_2Cu_3O_{7-x}$, $Y_{0.6}Pr_{0.4}Ba_2Cu_3O_{7-x}$) have been widely applied as barriers in different geometries also as Ga-doped samples which demonstrated $R_nA \sim 10^{-8} - 10^{-7}\ \Omega{\cdot}cm^2$. The barrier thickness changed into range of 6–30 nm, causing different values of critical current density, J_c. The value of I_cR_n changed linearly with the barrier thickness from 0.8 upon to 5 mV. At the same time, Ga-doped junctions demonstrated lesser sensitivity to changes of the barrier thickness.

Based on the barrier properties, the transport characteristics of the junction could be investigated. For instance, the behavior of PBCO bulk samples is defined by relatively high density of localized states, and PBCO-barriers allow ones to investigate effects of two localized states in inelastic process of tunneling [1814]. Moreover, *a*-axis YBCO–PBCO–YBCO junctions have been created on (100) $LaSrGaO_4$ substrates [1651] and on vicinal substrates (001) $LaAlO_3$–$SrAl_{0.5}Ta_{0.5}O_3$ [953] with spread of I_c and R_n equals to 11 and 8.8 %, respectively. It has

been stated that Josephson behavior takes place for barriers with thickness of 80 nm and coherence length of order 20 nm.

2.5.2.8 Interface-Engineered Junctions

These junctions have thin barrier layer, as rule on ramped edges created due to damage of surface of the YBCO-ground electrode at ionic bombardment [1175]. During following deposition of counter-electrode occurs recrystallization of the surface. This technology has been applied in order to create three-layered *c*-axis YBCO-specimens [1176, 1846]. The studies of the processed high-quality interface engineered junctions with magnetic modulation of the critical current upper 80 % and critical current density $J_c = 10^2 - 10^6$ A/cm^2 at $T = 4.2$ K confirmed that they could be considered as an array of microscopic S–N–S junctions, introduced in isolating barrier of arbitrary orientation. This filamentary structure corresponded to special orientations and, in particular prevented to effects proper for *d*-wave paring symmetry.

2.5.2.9 Junctions Based on Other HTSC

HTSC which are different from YBCO family also used due to their special properties. For example, the compounds, based on Bi and Ta, with their great anisotropy are preferable for natural junctions. YBCO-junctions, doped by Ca, exploit a property of excessive doping of the sample, at the same time electron-doped compounds can display new physical aspects. Majority HTSC compounds demonstrate dominating *d*-wave symmetry of order parameter. Presence of additional sub-dominated components could be depended on material and geometry of interface.

2.5.2.10 $La_{1.85}Sr_{0.15}CuO_4$-Based Trilayer with One-Unit-Cell-Thick Barrier

Most significant step on way of processing HTSC trilayer structures with insulating barrier became creation of structure consisting of $La_{1.85}Sr_{0.15}CuO_4$ (LSCO) electrodes divided by barrier of La_2CuO_4 (LCO) with thickness of one elementary cell [167]. This achievement was to be a sequence of intensive studies of BiSrCaCuO (Bi-2212) structure in previous years [1755]. Then, it has been discovered "giant" proximity effect in LSCO-junctions [168], observing Josephson current in samples with LCO-barrier of thickness from 1 up to 15 elementary cells (upon to 20 nm), that is far greater than the coherence length and mean length of free run of electrons. This result could not be understood into framework of classical theory. The authors assumed that the superconductive current was averaged at resonance tunneling through a set of energetically ordered states inside barrier layer. These experiments used transformation of junction from S–N–S to S–I–S type due to

low-temperature annealing in vacuum (that introduced an isolating state of LCO, practically preserving intactness of LSCO). Long-length or anomalous proximity effect has been also studied in another types of junctions and into framework of quantum phase transition between insulating antiferromagnet phase with low concentration of carriers and metallic or superconductive phase with high concentration of carriers [349].

2.5.2.11 Electron-Doped HTSC

Bicrystal junctions are most common type of junctions which includes electron-doped cuprate superconductors. As it has been stated in [115], the barriers in electron-doped compound $La_{1.85}Sr_{0.15}CuO_4$ possess in mean by lesser transmitted capability compared to YBCO-bicrystals demonstrating $J_c = 6{\cdot}10^3$ A/cm^2 at $T = 4.2$ K, $R_nA = 5{\cdot}10^{-8}$ Ω·cm^2 for misorientation angle of 24°, and $J_c = 3$ A/cm^2 at $T = 4.2$ K, $R_nA = 10^{-6}$ Ω·cm^2 for misorientation angle of 36°. The same technique which was used for YBCO-specimens allowed one to process zigzag-like junctions of ramp-edge type based on $Nd_{2-x}Ce_xCuO_{4-y}$ (NCCO). Then, the samples as optimally doped ($x = 0.15$) as with excessive doping ($x = 0.165$) have been prepared [55], which had double layer with thickness of 150 nm (001)-oriented NCCO and 35 nm $SrTiO_3$ (upper electrode was 160 nm Nb). As barrier have been used sub-layers of 12 nm NCCO and 12 nm Au. In the case of optimal doping were attained values of $J_c = 30$ A/cm^2 and $I_cR_n = 30$ μV at $T = 4.2$ K. Due to this the Josephson penetration depth $\lambda_J \approx 65$ μm turn out to be compared with the length of the zigzag face, and the resistance value was $R_n \approx 10^{-6}$ Ω·cm^2. By this, there were observed anomalous controlled magnetic images which witnessed on dominating *d*-wave symmetry without any alterations of *s*-wave at low temperatures.

2.5.2.12 Ca- and Co-doped YBCO and Overdoped Regime

As it has been shown in [627], an increasing critical current in bicrystal junctions was attained by using excessive doping of superconductor, in particular due to Ca- and Co-doping of YBCO-samples [331]. The latter samples of HTSC-junctions demonstrated best results in increasing J_c. The critical current has been studied in dependence on concentration of Ca demonstrating optimal doping at $x = 0.3$. Then, it has been defined $J_c = 7{\cdot}10^6$ A/cm^2 at $T = 4.2$ K for 24°-misorientation angle of grain boundary [1501], that is almost on order of magnitude greater than in the case of absence of the doping.

2.5.2.13 Ultra-Thin Films and Superlattices

Josephson junctions consisting only of several superconductive planes of CuO_2 (in particular, of 6 layers) have been processed on the base of ultra-thin $[Ba_{0.9}Nd_{0.1}CuO_{2+x}]_5/[CaCuO_2]_2/[Ba_{0.9}Nd_{0.1}CuO_{2+x}]_5/[CaCuO_2]_2/[Ba_{0.9}Nd_{0.1}CuO_{2+x}]_5$ (CBCO) structures 5/2/5/2/5). By this, the CBCO-film had thickness of only 8 nm. The Josephson effect has been measured even in junctions with wide of 5 mm [1640].

2.5.2.14 Intrinsic Stacked Junctions

Strongly anisotropic layered crystallite structure of cuprates allows creation of intrinsic stacked junctions, which are processed from bulk single crystals (see Fig. 2.15). Superconducting current in these junctions flows along of *c*-axis. Best results have been attained for single crystals and thin films of $Bi_2Sr_2CaCu_2O_8$ [887] and $Tl_2Ba_2Ca_2Cu_3O_{10}$ [888]. In *a*-axis oriented thin films of YBCO, it has been stated the Josephson pairing between double layers of CuO_2, and majority of materials led themselves similar to the stacked S–I–S Josephson junctions with effective barriers of order of the space thickness between double layers of CuO_2 (1.5 nm). By this typical value of critical current was 10^3 A/cm^2. Volt-ampere characteristics (*I*–*V*) demonstrated great hysteresis and numerous branches corresponding to subsequent link of high-qualitative junctions. Then, the practical recommendations on processing the intrinsic stacked junctions have been developed with aim to total elimination of heating effects [1859]. However, nevertheless it is necessary a carefulness by analyzing volt-ampere characteristics at high voltage because of possible keeping the heating effects. Finally, it has been confirmed that macroscopic quantum tunneling takes place in natural junctions of BSCCO [756, 786].

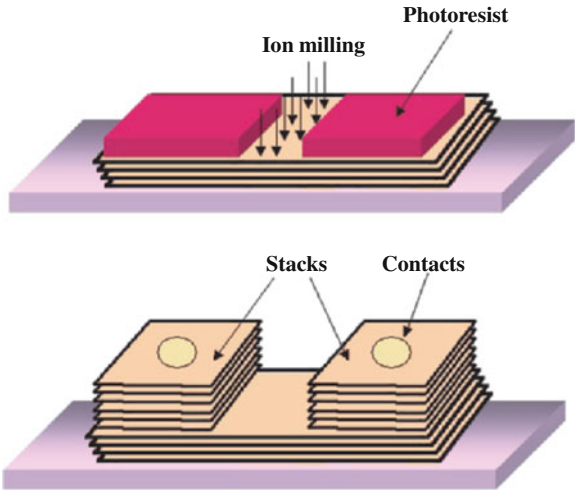

Fig. 2.15 An example of intrinsic stacked junctions. The mesas with *c*-axis transport are defined through mechanical etching [875]

2.5.2.15 Oxide Heterostructures

Development of technology of the growing multi-layer structures with atomic sharp boundary between the layers (for example by using molecular-beam epitaxy) allows one to create artificial material with advanced material demonstrating often very unusual properties. Especially great hopes are connected with oxides. For instance, while $SrTiO_3$ and $LaAlO_3$ are dielectrics, the interface boundaries in the $SrTiO_3/LaAlO_3/SrTiO_3$ heterostructure to be conductive, more that on the boundary of two insulating oxides has been discovered superconductivity [1427]. The characteristics of interfaces between cardinally different on their physical properties matters that as high-temperature superconductor $(Y,Ca)Ba_2Cu_3O_7$ and manganite $La_{2/3}Ca_{1/3}MnO_3$ with colossal magneto resistance have been studied experimentally and theoretically in [245]. It has been shown that due to the electric charge pass through interface, $d(3z^2 - r^2)$-orbitals of CuO_2 layers (which are totally filled in HTSC and do not take part in superconductivity) become to be filled only partially that is on them arise holes. This orbital reconstruction differs of usual electronic reconstruction which occurs on interfaces of other oxide compounds and consists in that what a distribution of electronic density near the interface differs of a volume distribution. This effect could be used to doping dielectric layers "no-chemical" method without effects of disordering, which are inevitably introduced non-isovalent admixture atoms. The practically important applications of this effect are connected, for example with magnetic tunnel junctions and "oxide electronics", one of directions of which to be R&D novel quasi-two-dimensional states (charge, spin, etc.), which in partially could be stabilized on the oxide interfaces.

http://www.springer.com/978-3-642-34440-4

Microstructure and Properties of High-Temperature Superconductors

Parinov, I.A.

2012, XXI, 779 p., Hardcover
ISBN: 978-3-642-34440-4